INTRODUCTION

The clustering of water molecules in the vapour phase plays an important role in many processes. Nucleation of water droplets, the beginning of the phase transition between vapour and liquid water, starts when clusters have grown large enough to pass the critical cluster size. It has been proposed that clustering of water molecules in the atmosphere plays a role in absorption of solar radiation[1].

Of special interest in the field of materials science is the role of molecules clustering during the diffusion of water through hydrophobic polymers, like polyethylene. This process has been studied by means of molecular simulation[2], and it was shown that the molecules did not diffuse through the polyethylene in the form of monomers. Instead, the water molecules form clusters in the polymer, between which the single molecules made jumps. The structure of water in polyethylene is of interest in the formation of water trees under the influence of a high voltage field. The molecular mechanisms behind water tree formation and the subsequent polymer degradation are not fully understood, but as is indicated by the name, the voids and channels that build up a water tree contain water (cf, Figure 1).

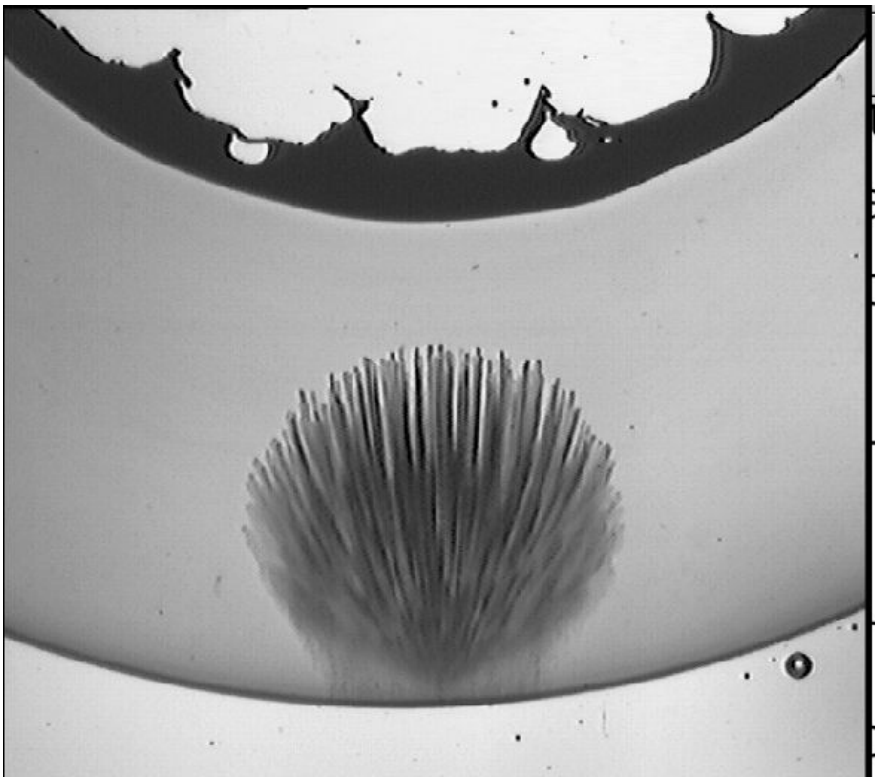

Figure 1: Water trees can be seen as tree- or bush-like structures built up by paths of small water containing voids, or in more severe cases, channels in the polymer.
(Published with permission from B. Holmgren, ABB, Västerås.)

WATER TREES

These water trees tend to form in polymer used for high voltage cable insulation purposes where it can cause insulation failure[3]. Water trees are macroscopic tree- or bush-like structures built up of paths of water-filled voids with radii from 1μm to 5μm. In more severe cases these paths of voids form larger channels in the polymer. Water trees appears after long service life, and the phenomenon was reported[3] in 1972, years after polyethylene was first used as high voltage insulation material during the 1960's.

As mentioned, the voids forming a water tree are filled with water and the deformation of the polymer is permanent. If a water tree is dried out and later exposed to water again the water tree will reappear[4]. Necessary conditions for water tree initiation and growth are the presence of water and an alternating current (AC) field. The presence of ions also seems to be important, since it is very difficult to grow water trees experimentally if the polymer is not in contact with ions. Bulinski et al.[4] have performed experiments on water tree initiation on samples saturated with salt solution. They found that water tree densities were similar for both NaCl and $CuSO_4$ solutions, and that the water tree initiation rate was not affected by the presence or absence of oxygen, suggesting that oxidation is not a major factor in the water treeing mechanism. Other elements detected in water trees[5] are Fe, Al, S, K, C, Cu, Si and Ca.

Water trees have been reported to grow[5] at external fields as low as 1.9×10^6 V/m. This is much lower than the electric field that insulation is typically exposed to, which is approximately $10^7 – 10^8$ V/m. Defects in the electrically conducting metal, such as asperities, or impurities in the polymer, are expected to create local electric fields that are larger than 10^8 V/m (Ref 6). A study performed by Radu et al.[7] concluded that the presence of water in water trees increases the permittivity compared to unaffected regions, which enhances the local field. According to the latter investigators, a water tree can have a local self amplification of as much as 50% of the external field at the extremities of the tree. These effects, that enhance the external field from the condcutor are crucial for the insulation breakdown mechanism since the growth rate of water trees is a linear function of the applied field[5].

Knowledge of the breakdown mechanism of the polymer on a molecular level would be of great benefit in the design of voltage stabilizers for use in polymers for high voltage insulation purposes. There are many studies that support that the breakdown mechanism is a mechanical process, at least

in its initial stages[8,9]. That is, the water found in the water trees does not arise due to chemical reactions in the polymer. Instead, the appearance of water in the water tree voids indicates that water diffusion and solubility play a crucial role in this breakdown mechanism.

SIMULATIONS OF PURE WATER

APPENDED PAPERS I AND II

MOLECULAR SIMULATION METHODS

There are two common methods used in classical molecular simulations, the molecular dynamics (MD) method and Monte Carlo (MC) methods. In MD simulations Newton's equation of motion is applied to the atoms or molecules, which have a mass and a kinetic energy. The evolution of the system is solved for a short time step, we get a new configuration, and this is then repeated for many time steps until the desired simulation time has been reached. This method is suitable for studying the time evolution of systems, but since simulations cannot be longer than nanoseconds, with today's computers, equilibration processes are difficult to study with this method. Molecular dynamics is very suitable for studies of, for example, diffusion, relaxation (when the relaxation time is short) and nucleation.

The second, Monte Carlo, method is a statistical approach. Monte Carlo involves several different methods that have one thing in common, i.e, Monte Carlo methods make extensive use of random numbers, every action taken to the system is decided randomly, and the change to the system is then accepted or rejected according to the change of potential energy in the system that the action causes. Time is not involved in Monte Carlo, instead every configuration can be considered as a possible structure at equilibrium conditions. Since there are an almost infinite number of possible configurations, one cannot draw any conclusions from a single MC configuration. Instead a lot of configurations are created and the property that is of interest is obtained as an average from all generated configurations. This method is suitable for the study of systems that are in equilibrium, like phase coexistence in mixtures.

Water clusters have previously been studied with both MD (for example nucleation rates, vibrational frequencies and lifetimes) and MC methods (for example size distributions, topologies and critical cluster sizes). Most MC studies of water clusters have employed the Grand Canonical

Monte Carlo method where the system's temperature, volume and chemical potential are fixed. Molecules can be inserted, and allowed to escape from the system so the density (number of molecules in the simulation) of the system can be said to be in equilibrium at the chemical potential used. Unfortunately, the chemical potential is imposed on the system so the result will be affected if it is wrong. There is a method that can get around this problem though, and let the chemical potential adjust itself to its equilibrium value. This method is called the Gibbs ensemble.

GIBBS ENSEMBLE

The Gibbs ensemble method is a Monte Carlo simulation method proposed by Panagiotopoulos[10] in 1987. The method employs two different boxes, one containing the first phase (e.g. liquid) and the other containing the second phase (e.g. vapour). It is normally difficult to simulate coexisting phases due to the interfacial effects. Consider a cube consisting of 1000 molecules. It has 488 surface molecules and a smaller system has an even higher fraction of molecules located on the surface, so a system has to be very large in order to be able to reproduce bulk properties. Both boxes in a Gibbs ensemble simulation are filled with bulk matter and there exists no interface between them. Hence there are no surface molecules in the system. The boxes are connected to each other by the possibility to transfer molecules from one phase to the other. The temperature, pressure and chemical potential are equal in the two boxes, as it is on a macro-scale between different phases in nature.

As illustrated in Figure 2, there are some different types of actions taken to the system during the simulation:

- Particle moves within one box of two types, translation and rotation of particles. Also methods that combine the two actions exists.

- Volume changes, where one box is scaled down to a smaller size at the same time as the other box is scaled up. It is a pure transfer of volume between the boxes, so that the total system volume is kept constant. Systems with two or more components can also be studied with fixed pressure, instead of fixed volume.

- Swap moves, where a particle is inserted into one box at the same time as another particle of the same type is deleted in the other box. This allows for the densities of the phases to adjust to equilibrium values.

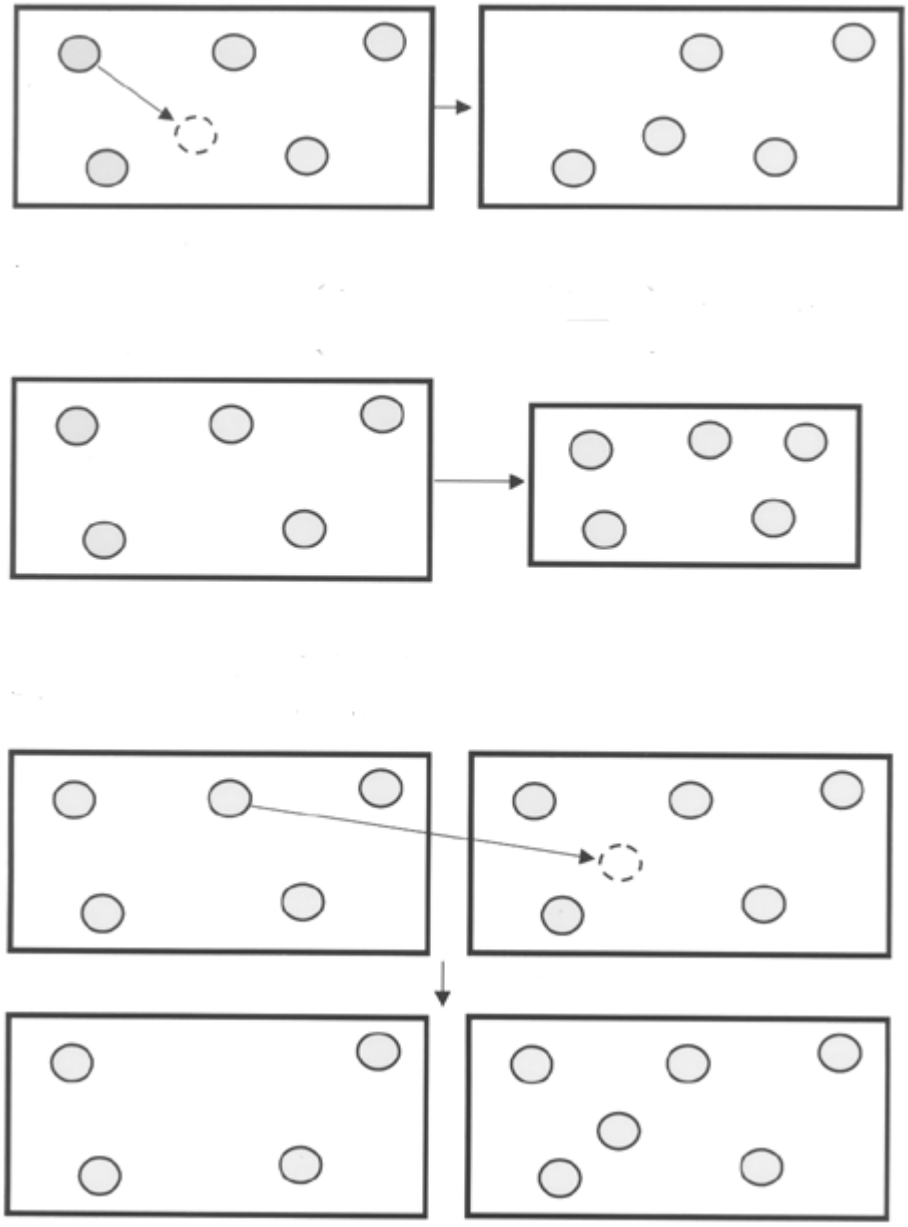

Figure 2: During the Gibbs ensemble simulation run, three main types of changes are applied to the system, translation of molecules, volume exchange between boxes and swap moves where one molecule is inserted into one box at the same time as another is deleted in the other box.
(Published with permission from T. McKnight, University of Natal, Durban.)

As mentioned above, both boxes contain bulk matter, and this implies that there are no boundaries at the edges of the simulation boxes. This is taken care of by the use of periodic boundary conditions, which means that the box is considered to be surrounded by identical copies of itself in all directions. Intermolecular interactions are calculated between one molecule and the copy of another molecule that is found to be closest, regardless of if it is situated inside or outside the simulation box. When a particle is transferred out of the box in any direction, a copy of the particle is transferred into the box from the opposite direction.

Ideally, two boxes of the same size are initially filled with an equal amount of molecules. The initial size of the boxes are determined by the number of molecules used in the simulation. Once the total number of molecules has been selected, an approximation of how many of these molecules will be in the vapour phase box at equilibrium and at the temperature of interest is made. The volume these molecules would occupy, both in the liquid and vapour, is then calculated from experimental densities (or approximated if experimental data is not available). Since the result of this procedure is a density between the real vapour and liquid densities, this is not an equilibrium state. In the initial configuration the molecules have been inserted at random positions and with random orientations, so this configuration is most likely a very unfavourable, high energy configuration. The system thus has to be equilibrated for more than ten thousands of Monte Carlo cycles with only translational and rotational moves. A Monte Carlo cycle involves an equal number of actions taken to the system as there are molecules in the system. It is from the resulting configurations after each completed Monte Carlo cycle that the properties of interest are sampled. More favourable positions and orientations for the molecules are achieved after the equilibration, but the system will still be metastable since the densities do not conform with the stable liquid and vapour densities. The next step is to allow for swap moves and volume exchanges. The system will now rapidly change when phase separation takes place, a lot of molecules will be swapped from one box to the other and one vapour and one liquid phase will be formed in only a couple of hundred MC cycles. When the densities have stabilized is it time to start sampling the properties of interest.

The events described above do unfortunately only apply to systems with small molecules and when no charges are involved, like shorter alkanes. If a molecule is large there is a low probability that an insertion trial into the liquid will get accepted. The same applies to molecules with charges, like water, since the molecules in the liquid phase are quite well oriented due to the hydrogen bonding and the probability for an accepted insertion is relatively low. This means that the equilibration time will be several times longer than previously described. One way to get around this problem, in the

case of water simulations, is to start the simulation with initial densities in the boxes relatively close to experimental values. Even with this approach the equilibration time is at least 100 000 MC cycles. The long equilibration time for water is in fact the upper limiting factor to the system size, and an increase in the system size by a factor two, increases the computation time by approximately an order of magnitude. The equilibration of a 500 water molecule system takes about two days on our computers, with a performance similar to most modern PC's, so already a system of 2000 molecules would occupy a computer for more than half a year, only with the equilibration.

The lengths of the production runs range between 30 000 and 3 000 000 MC cycles and have been determined by the amount of molecules that were predicted to be present in the vapour phase, and consequently that the anticipated number of clusters were sufficiently large for statistical analysis.

The use of the Gibbs ensemble method in this study means that the major part of the computations have been used to calculate interactions in the liquid, especially at the lower temperatures. The liquid density at e.g. 300 K is 10 000 times higher than in the vapour, but Gibbs ensemble is the only molecular simulation method where we can be sure that vapour and liquid are in true equilibrium with each other.

THE SPC/E MODEL AND INTERMOLECULAR INTERACTIONS

The SPC/E model[11] is an empirical three site water model with a Lennard–Jones (L-J) energy parameter (ϵ) of 0.649 kJ/mol and a point charge of –0.8476 *e* situated on the oxygen, and positive point charges of 0.4238 *e* on each of the hydrogens. The rigid hydrogen–oxygen–hydrogen angle is 109.5° and the oxygen–hydrogen distance is 1.0 Å.

The formula for the intermolecular Lennard–Jones 12–6 potential energy is as follows;

Equation 1:

$$\upsilon^{LJ}(r) = 4\epsilon((\sigma/r)^{12} - (\sigma/r)^{6})$$

where *r* is the distance between the L–J sites. The potential is repulsive at distances shorter than $2^{1/6}\sigma$, ($\approx 1.122\sigma$), attractive at all distances longer than $2^{1/6}\sigma$, and it has a minimum, with well depth ϵ, at a distance of $2^{1/6}\sigma$. This minimum would be the equilibrium intermolecular distance if no charges were involved. The intermolecular oxygen–oxygen distance (σ) where the Lennard-Jones potential is zero between two SPC/E molecules is 3.166 Å. A cut–off distance in the intermolecular interactions has to be used since periodic boundary conditions are used, which means that the

system looks the same in all directions on a scale of many boxes in every direction. It is also necessary to restrict the number of calculated interactions for the reason of computational performance. A cut–off distance of 9 Å has been employed, which is safely below half of the box lengths at all circumstances, so that the risk of contributions to the intermolecular energy between molecules in the box and their periodic images is eliminated. The energy contribution from molecules located outside of the sphere is taken care of with a tail correction integral that assumes that the density of the system is the same outside as inside of the sphere[12]. Electrostatic interactions have a longer range than the cut–off radius, and Ewald summation[13] has been employed to take care of the long-range contributions to the potential energy. This is a (rather complicated) method to compute the contributions from point charges in systems with periodic boundary conditions. As mentioned, the potential between point charges decays so slowly that a charge at one box length's distance makes a considerable addition to the potential energy. Because of this slow decay in potential energy, imposing a cut-off radius is not an accurate assumption. However, when one does not impose a cut-off radius the molecule's periodic images would create a background field, uniform in all axis directions, since the distance to a molecule's periodic images in all the surrounding boxes is the same. The Ewald summation is also a rather computationally costly method, and a performance analysis of the simulation program has shown that the subroutines involved in the Ewald summation consumes approximately 90 % of the CPU time.

The SPC/E model was proposed by Berendsen in 1987, and it has been used in hundreds of molecular simulation studies. Boulougouris, Economou and Theodorou[14] have in a Gibbs Ensemble Monte Carlo (GEMC) study shown that the SPC/E model predicts the radial distribution function of the liquid in good agreement with experimental data, and that the saturated vapour densities are similarly close to experiment as those obtained from the MSPC/E[14] model, and closer than the SPC model[15]. Other GEMC studies by Errington and Panagiotopoulos[16] and also by Economou[17] show that the SPC/E model yields vapour densities similar to the EP-6 model[16]. In a MD study done by Mark and Nilsson[18] they conclude that SPC/E gives a radial distribution function in better agreement to experiment than TIP3P (Ref 19) and SPC. Cummings and co-workers[20] have compared the 3-dimensional liquid structure of SPC, SPC/E, MSPC/E, TIP4P, TIP5P (Ref 21) and polarizable point charge[22] (PPC) models and found that SPC/E and TIP4P produced a better ordered structure than SPC and MSPC/E, but less ordered than TIP5P and PPC. Hayward and Svishchev[23] have shown that SPC/E replicates the vapour-liquid equilibrium curve better than the polarizable point charge (PPC) model. Lísal, Smith and Nezbeda[24] have done a GEMC study of

TIP4P water. From their results it can be concluded that TIP4P overestimates the vapour density at all temperatures (SPC/E underestimates vapour density, but is closer to the experimental vapour-liquid equilibrium curve), and the critical temperature is 59 K lower than experiment. A comparison of the TIP4P, TIP5P and TIP5P/E (Ref 25) models by Lísal et al.[26] showed that the two TIP5P models are inferior to the TIP4P model for vapour-liquid equilibrium properties. Other comparisons indicate that the SPC/E model reproduces other properties of water as well, if not better, than other simple water models[27-29].

One great advantage with the SPC/E model in the long simulations performed in this study is its simplicity, since the computational cost grows exponentially with the number of sites in the molecules, and most other models have four or more sites.

CLUSTER DEFINITIONS

Analysis and discussion of (water) clusters may be very sensitive to the way in which the cluster is defined, so it is very important to be clear about what kind of cluster definition has been used. The first type of definition that has been used in cluster studies is a pure distance criterion, proposed by Stillinger in 1963[30]. If the distance between two molecules is shorter than a certain cut-off distance, the molecules are considered to belong to the same cluster. In the case of water studies, an oxygen-oxygen cut–off distance of 3.8 Å has been commonly used. In my studies have I used a slightly larger cut-off of 4.0 Å. A smaller cut–off of 3.8 Å has also been tested to check if this difference affects the results, and the difference in the results is very small. The reason for the modified distance criterion is because a cut-off of 4.0 Å will always include the whole first peak in the oxygen-oxygen radial distribution function, regardless of temperature. Since this definition does not in any way consider the orientation of the molecules, it might be considered as a little bit unsophisticated for water molecules, where molecular orientation is important.

A more advanced cluster definition is to consider two molecules as members of the same cluster if there exists a hydrogen bond between them. Several different types of definitions of a hydrogen bond have been proposed, where the oldest are based only on an energy criterion, where bond energy levels between -5.45 and -18.85 kJ / mol has been used. Other hydrogen bond definitions are based on a composite criterion of both distance and energy, or in some cases bond angle. The definition used in this study has been proposed by Kalinichev and Bass[31] and consists of a cut-off

distance between the oxygen on one molecule and a hydrogen on another molecule of 2.4 Å and also an intermolecular energy less than -10 kJ / mol. This definition has been used to study clustering of supercritical water[31], though not with the SPC/E model.

CLUSTER ANALYSIS

During the simulations the coordinates for vapour molecules at every configuration have been saved on disk, together with the vapour box size. The data have subsequently been run through an analysis program, which has first searched for physical clusters by means of calculating the oxygen-oxygen distance between the different vapour molecules, i.e. physical clusters refer to those clusters defined using the pure oxygen–oxygen distance criterion. Since each pair of hydrogen bonded molecules (with the definition mentioned earlier) will also pass the criterion for membership in physical clusters, all physical pairs have been stored in memory in order to get a shorter list of pairs for the much more computationally expensive hydrogen bond calculation.
The molecule numbers (used to identify the molecules by the program) in the pairs have then been compared to determine if a particular molecule occurs in more than one pair. If this is the case, then the molecule belongs to a cluster that is larger than a dimer. It is in this way determined how many different clusters (and their size) are present in each configuration.

To determine if a hydrogen bond exists between water molecules is a much more computationally costly task than determining if they are physically bonded, since not only the distance, but also the intermolecular energy has to be calculated. The intermolecular energy (for SPC/E water molecules) consists of two different parts, the Lennard-Jones energy between the oxygen sites of two molecules and the electrostatic energy between all the charges on each molecule. Since there are three charges on each molecule, and consequently nine electrostatic interactions to be calculated between each pair of molecules, we get a total of ten energetic interactions that has to be summed up for each pair tested.
The hydrogen bonded clusters have not only been studied regarding cluster size, but also the radius of gyration, the average number of hydrogen bonds per molecule and the topology of smaller clusters have been considered. The average number of hydrogen bonds can easily be determined when the number of molecular pairs in a particular cluster and the size of the cluster are known. The topologies, which have been analysed for trimers, tetramers and pentamers, can be determined when

it is known in how many pairs each molecule occurs. In some cases it is also necessary to consider in how many hydrogen bonds the neighbouring molecules are involved. It is then possible to classify which type of topology the cluster has. There are two possible topologies for a trimer, six for a tetramer, and 20 for a pentamer, even though several of the tetramer and pentamer topologies are energetically very unfavourable and will not be found very frequently. The rapid increase in possible topologies with increasing cluster size makes it a bit difficult to do this analysis on larger clusters than pentamers. Even though it is difficult to explicitly determine the topology of hexamers and larger clusters, it is still possible to get an idea of the structure of a typical cluster of a certain size from the average number of hydrogen bonds per molecule, where a cyclic cluster has the same amount of bonds as there are molecules, a linear cluster (with or without sidebranches) has less than one hydrogen bond per molecule. If the number of bonds is larger than the number of molecules then the cluster contains more than one ring. Another reason that we have not studied the topologies of clusters larger than pentamers is that the minimum energy topologies of hexamers and larger clusters differs between the SPC/E model and results from quantum mechanical calculations[32].

It is also possible to get an idea of the shape of the clusters from the radius of gyration. If a chain is grown with a self – avoiding random walk mechanism, we will get an increase in the radius of gyration close to $n^{0.6}$. The exponent will be higher if the shape of the cluster is more straight and we would get an exponent of $n^{0.33}$ if the cluster forms a sphere.

COMMENTS ON THE METHODS AND RESULTS

Most of the results are presented in the papers, and are for that reason not further discussed here. However, some details about the methods, and hence some results, might be worth mentioning here.

The study has been performed at temperatures between 300 K and 600 K, but the only place where the lowest temperatures, 300, 315 and 333 K, appear is in the vapour – liquid equilibrium (VLE) diagram. Why? And why have not temperatures even closer to the triple point (273 K, for real water) and the critical point (630 – 640 K, for SPC/E) been examined? The answer is, in the case of the lower temperature limit, that a study at lower temperatures would be meaningless with computers that are available today. Of the 3 000 000 Monte Carlo cycles run at 300 K only 32 had more than one molecule present in the vapour box, half of those configurations contained a dimer.

Approximately 2 996 000 configurations were empty, i.e. there was no molecule at all present in the vapour box. It is first at 350 K that the vapour gets dense enough, so that the amount of clusters is large enough to give reasonably reliable statistics. More than 4 000 clusters were found at 350 K.
The temperature ranges in the appended Papers I and II differ in their upper limits. The papers are both based on the same simulation results (i.e. configurations, which can be used for different types of analyses). It was decided to extend the study to 600 K at a relatively late stage when Paper I was already written, since it was seen that clusters were very abundant in the vapour at higher temperatures.
Note that the radial distribution function in Paper II shows that the average density at a distance of 2.8 Å from an oxygen is more than 100 times higher than the average density in the vapour box at 350 K. The tendency for molecules to cluster is even higher at lower temperatures; the peak in the radial distribution function at 300 K reaches 800 times the bulk density, but one has to be aware that the statistics is poor at that temperature.
The average number of clusters per configuration increases rapidly with increasing temperature (see Figure 1 in Paper I, Figure 3 in Paper II), and reaches eight at 600 K. Hence shorter simulation lengths can be used to get statistically converged results at higher temperatures. The time it takes to perform a simulation is similar regardless of the number of molecules in the vapour box, since the total amount of molecules in the simulation is the same. It took approximately two months to perform a simulation with the length of 3 000 000 Monte Carlo cycles for a 500 molecule system, and a 1 000 molecule system would have required two years of CPU time. Since it would be unrealistic to wait such a long time for results, the simulations of the large systems have been divided into 10 different runs on separate processors, all based on the same equilibrated configuration, the only difference being different random number seeds.

The reason that the upper temperature limit in the study is 600 K is that there is a limitation in the Gibbs ensemble method that restricts the usable temperature range to temperatures where there is a large difference between the liquid and the vapour density. If the density difference is too small between the boxes there is a large probability that a lot of molecules gets swapped from one box to the other randomly and this might cause an identity change between the boxes. The former liquid box becomes the new vapour box and the corresponding has happened to the other box. This occurrence means that any statistics sampled during the simulation is unreliable, especially as it might happen more than once during a simulation run. The Gibbs ensemble method gets more and

more unreliable as the temperature approaches the critical temperature of the substance (where the density difference between the phases are small). There is a risk of box identity swaps even at 600 K, but it did not occur during the simulation in this study.

As can be seen in Figure 6 of Paper II, there is a strong indication of a structural transition in the topology of both tetramers and pentamers, even though it appears to happen at a temperature below 400 K. The number of observed tetramers and pentamers are low at lower temperatures, so it is not possible to draw any conclusions about the exact temperature for the structural transition from the simulation results.

It is, however, possible to calculate several properties from the plots of the fractions of different topologies by the use of some formulas from chemical thermodynamics. The change in Gibbs energy can be calculated as follows;

Equation 2:

$$\Delta G = - RT\ln K$$

where R is the gas constant, 8.31 $Jmol^{-1}$ K^{-1}, and K is the equilibrium constant for the particular reaction, in this case the transition from a cyclic to a linear topology. K is described by the concentration (in our case the fraction) of the products (linear clusters) divided by the fraction of the reactants (cyclic clusters). The Gibbs energy can also be described by;

Equation 3:

$$\Delta G = \Delta H - T\Delta S$$

where ΔH and ΔS is the change in enthalpy and entropy respectively. So, if we combine the formulas and rewrite them we get;

Equation 4:

$$\ln K = \Delta S/R - \Delta H/RT$$

Ln K is plotted against $1/T$ in Figure 3, and the slope of the curve equals $\Delta H/R$, and consequently there is an energy difference of 28 kJ / mol between cyclic and linear tetramers. Since there is a difference of one hydrogen bond between a cyclic and a linear tetramer this energy difference should indicate the hydrogen bond energy of SPC/E water. This is very close to the minimum intermolecular energy between two SPC/E molecules of 30.0 kJ / mol reported by Chen et al.[33]

The fractions of cyclic and linear clusters are equal at the structural transition temperature i.e. $K = 1$ at this temperature. Since ln 1 is zero, an extrapolation of the curve to y = 0 gives us the transition temperature. The calculated transition temperature between cyclic and linear tetramers will with this method be 377 K.

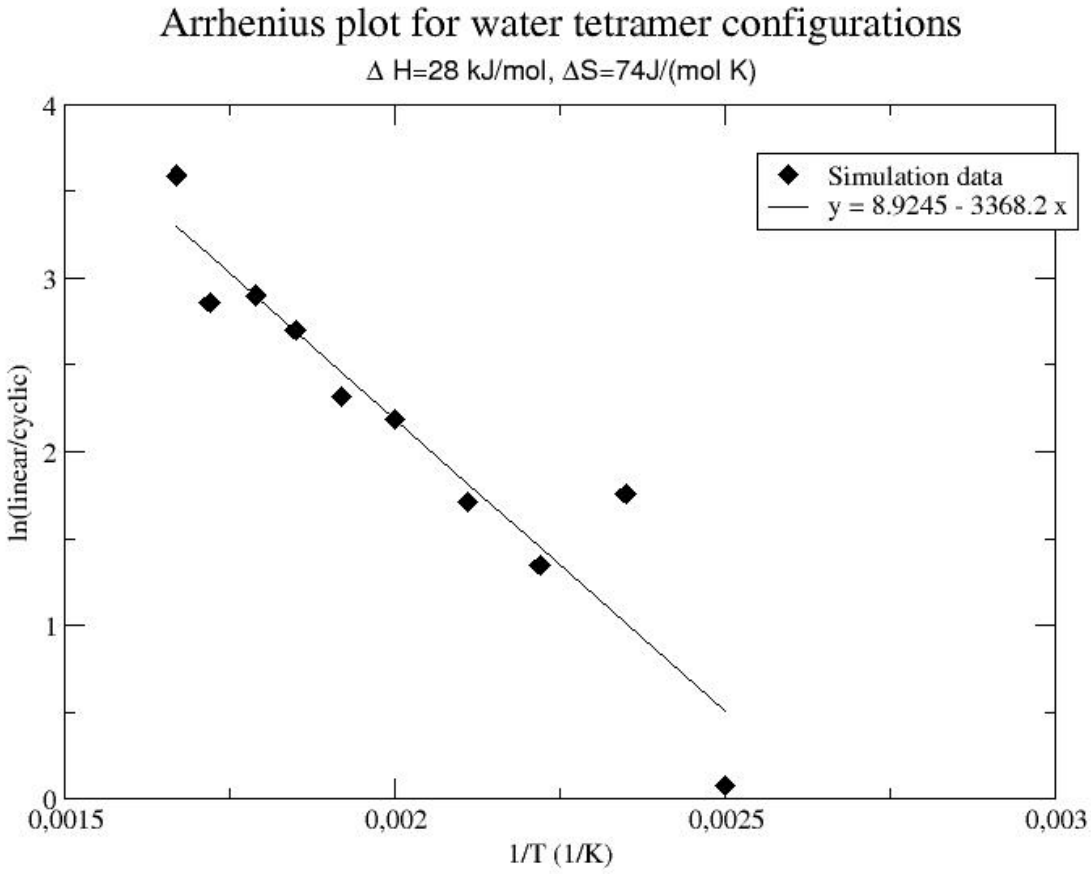

Figure 3: Plot of ln (fraction linear clusters / fraction cyclic clusters) vs. temperature^{-1}.

STUDY OF THE SPC WATER MODEL

This study is not included in the appended papers. It has been performed by Dr. Lennart Jönsson, School of Engineering, University College of Borås under my supervision.

The previously described study of SPC/E water has been repeated with the SPC model with the purpose to study model dependence on the results. The SPC/E model has been developed from the SPC model, and SPC/E reproduces liquid properties better than SPC, e.g. liquid density[14]. SPC/E also reproduces vapour densities better at temperatures above 500 K, but SPC produces results closer to experimental results in vapour for several properties such as densities at temperatures below 500 K, pressures and the second virial coefficient[14]. It is thus of interest to study the vapour structure using this model. The difference between the two models is that SPC has a smaller dipole moment, the model parameters are shown in Table 1.

The number of water molecules used in this study has been 200. This means that the liquid box length is smaller than 18 Å, which was the smallest possible box length in the previous study (two times the cut–off radius). This has been possible since the simulation program used in this study[34] does not employ a cut-off radius. Instead is it using the minimum image convention[12], which means that the interactions between a molecule and the nearest images of all other molecules is calculated. Hence the molecule is not located in the centre of a sphere, as when using cut–off radius, but in the centre of a cube instead. As a consequence of the cubic shape the long range correction calculation is more complicated, although it is not more computationally expensive[35]. This method is efficient on systems where the number of molecules in the simulation box is less than the number of molecules that would be located inside of the sphere formed by the cut–off radius. The efficiency decays quickly when the number of molecules in the simulation increases, since interactions have to be calculated between all molecules in the system. The possibility to simulate a system with only 200 water molecules, instead of 500 in the previous study, has made it possible to run more Monte Carlo cycles in shorter times. To study the effect of system size and truncation method, the SPC/E model has been employed on 200 and 500 molecules systems at 350 and 500 K. The simulations of the 500 molecules systems are not finished at the date of printing this thesis. Data for SPC/E 500 molecules systems are thus taken from the study presented in Papers I and II.

The temperature in the study ranges from 300 K to 500 K with increments of 50 K, and an additional highest temperature of 530 K. The reason that it stops at lower temperatures than the previous study is since the critical temperature[14] of SPC is around 590 K. A highest temperature of 550 K was tested, but the boxes switched identity at that temperature. An upper temperature limit of 530 K was thus chosen.

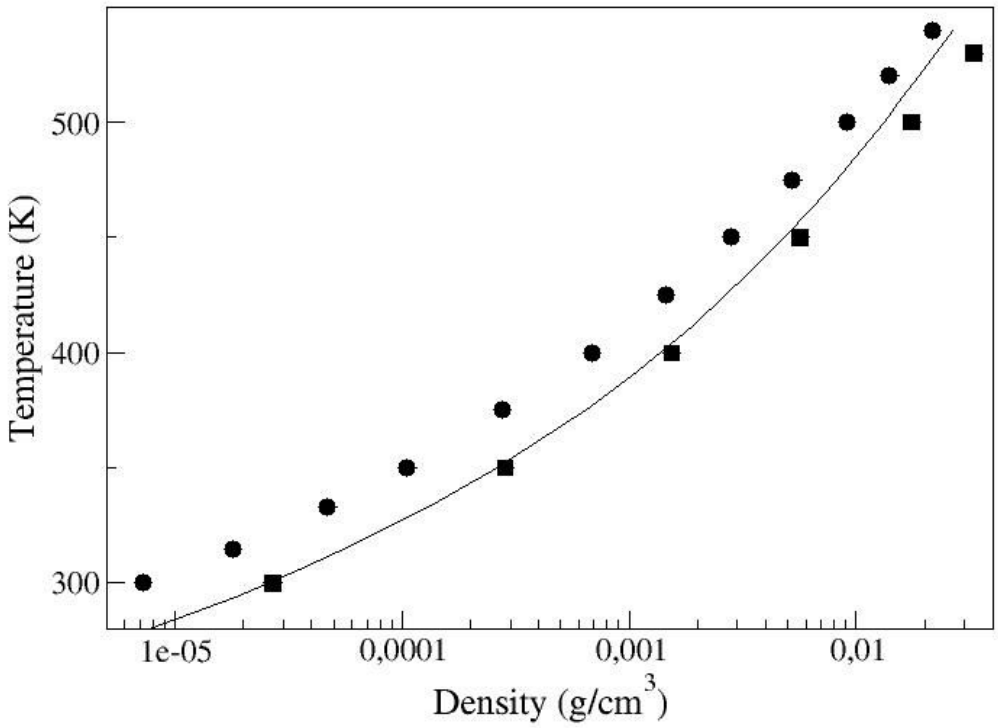

Figure 4: Water vapour densities. Data are shown for SPC/E, 500 molecule system, (circles) and SPC (squares). The solid line shows experimental data. Error bars for both models are much smaller than the symbols.

Figure 4 shows the SPC vapour densities from this study compared to the SPC/E vapour densities from Paper II and experimental data. Densities from the 200 molecules SPC/E simulations at 350 and 500 K are similar to the SPC/E densities shown. It is clear that SPC fits excellently to experiment at lower temperatures, and SPC gives better results at all temperatures up to 500 K. The lower vapour density for the SPC/E model is due to the higher dipole moment, i.e. the molecules 'prefers' to be in the liquid phase, where it has more neighbours.

The SPC/E vapour density at 300 K is only a quarter of SPC density at the same temperature and the SPC model yields results very close to the experimental density at the temperature. Even though the density of SPC vapour is close to experiment, the number of molecules in the vapour box is still too low to give any results on vapour clustering to report at that temperature. Figure 5 shows the number of clusters regardless of size as a function of total number of water molecules in vapour box. SPC shows the same trend as SPC/E in that there are always more physical than hydrogen bonded clusters and in that the number of clusters increases with increasing temperature. A difference between the models is that there are more vapour phase clusters when using the SPC rather than the SPC/E model. It could be expected that the SPC/E model would tend to cluster more with its higher dipole moment, but it is clear that the higher vapour density, and hence vapour pressure of SPC has a more pronounced effect than the lower dipole moment. That the clustering increases when the denstity increases has been shown in the appended papers. The difference between the SPC/E 200 and 500 molecules systems can be either due to system size effects or due to the different methods to calculate long range corrections.

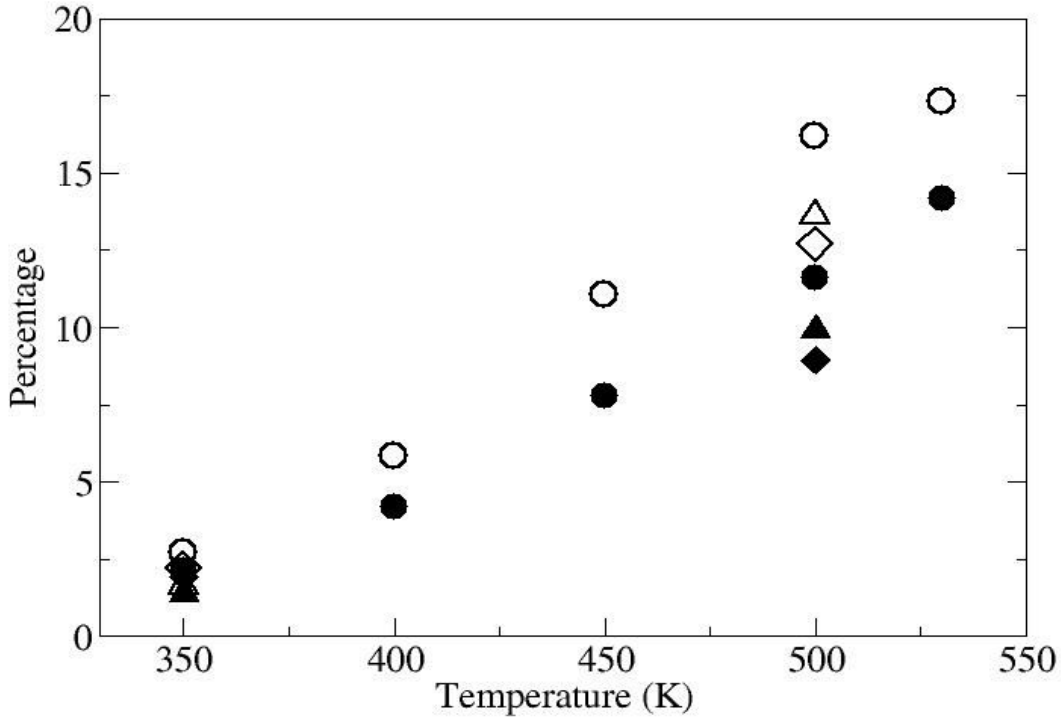

Figure 5: Percentage of physical (open symbols) and hydrogen bonded (filled symbols) clusters with respect to the temperature. SPC, 200 molecules system (circles). Results for SPC/E are shown as comparison, 200 molecule system (diamonds) and 500 molecule system (triangles).

The percentages of vapour molecules included in clusters with a size from dimers to pentamers are shown in Figure 6. The results at 350 K are very similar for SPC and SPC/E. At 500 K, on the other hand, the percentages of clustered molecules in all sizes of clusters are slightly higher for SPC.

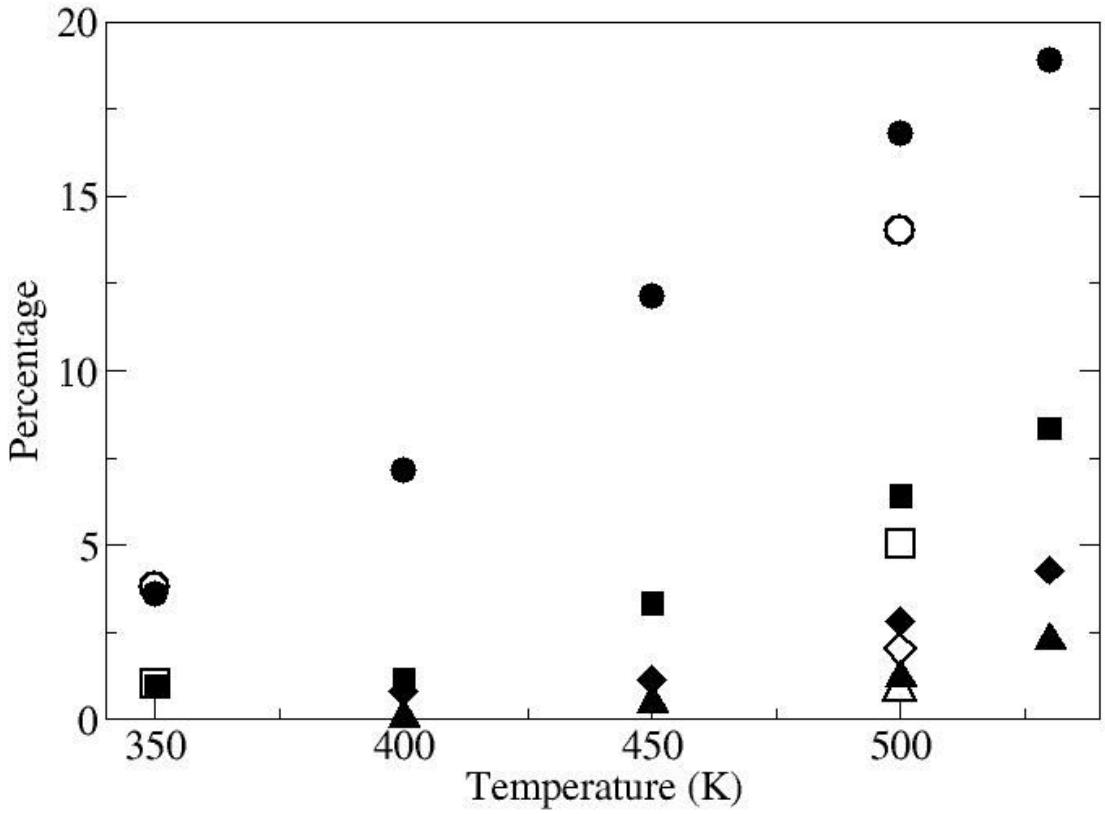

Figure 6: Fraction of water molecules included in hydrogen bonded clusters. System size is 200 molecules. Filled symbols are for SPC and open symbols for SPC/E (only 350 and 500 K). Dimers (circles), trimers (squares), tetramers (diamonds) and pentamers (triangles).

The topologies of SPC trimers differs from SPC/E in that the percentage of linear trimers is more or less constant at 95 % between 350 K and 530 K. The percentage of linear SPC/E trimers shows an increasing trend with increasing temperature. The percentage of the most common SPC tetramer and pentamer topologies shown in Figure 7 shows almost identical figures as for SPC/E at temperatures from 450 K and up. SPC/E is not shown for the sake of clarity, and the data is shown in Figure 6 of Paper II. One obvious difference is that the large fraction of cyclic tetramers found at 400 K for SPC/E is not seen for SPC. It should be noted that in one of the shorter simulation runs included in the study, a stable cyclic tetramer occured that lasted for thousands of Monte Carlo

cycles. This phenomenon has also been observed for SPC in simulations of water and hydrocarbons and is described in the appended Paper IV. The results from that simulation run has been deleted from the study and it can thus not be excluded that the fraction of cyclic tetramers is underestimated. Another difference compared to SPC/E is that the number of pentamers at 400 K is too small to give reliable statistics. Pentamers were only found in one out of eight simulation runs at that temperature, in contrast to the SPC/E simulations where the found pentamers were more evenly distributed over the different simulation runs. This is another indication that the SPC model has a stronger tendency than SPC/E to form stable clusters.

For SPC/E, only the four shown pentamer topologies, out of the 20 possible topologies, occured with an abundance of more than one percent at any temperature. Ten percent of the SPC pentamers had other topologies than those shown at 450 K but it is always the four topologies shown that are the most common.

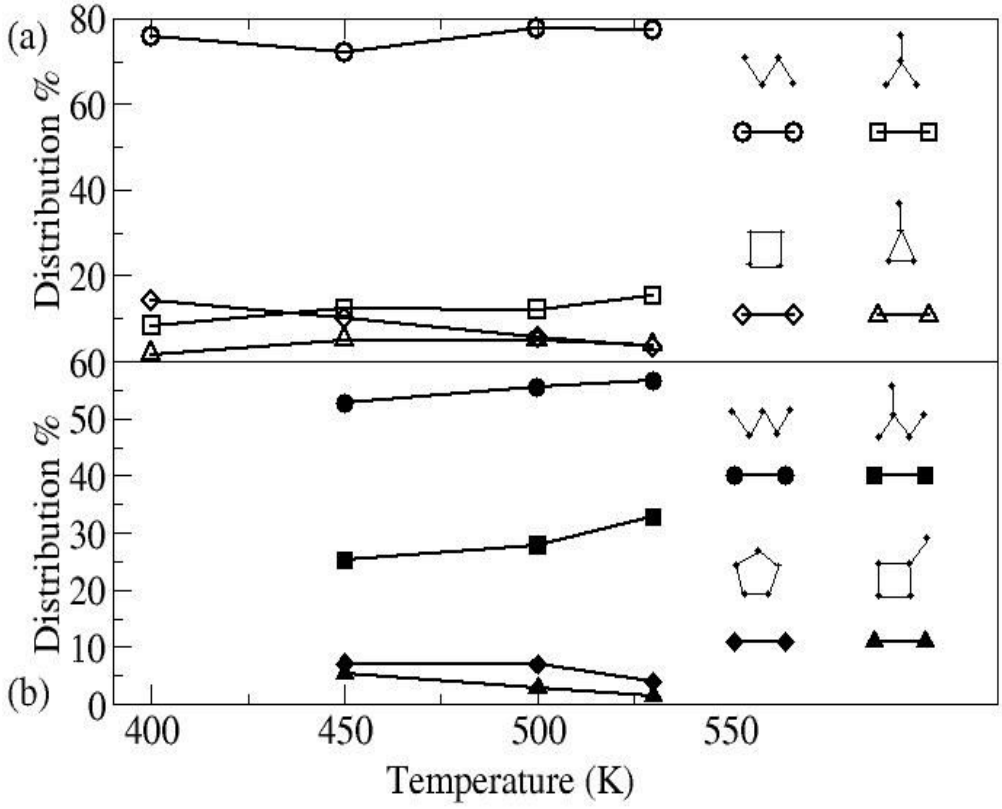

Figure 7: Percentage of the four most common SPC tetramer (a) and pentamer (b) topologies between 400 and 530 K.

Thank you Lennart!

SIMULATIONS OF WATER AND HYDROCARBONS

SOLUBILITIES AND STRUCTURE OF WATER IN N-ALKANES

APPENDED PAPERS III AND IV

The Gibbs ensemble study of water solubility and structure in n-alkanes ranges over hydrocarbon chain lengths from hexane (C_6) to hexadecane (C_{16}). The simulation temperature has been 450 K. Decane systems have also been simulated at different temperatures from 350 K to 550 K. Thus it is possible to study the effect of both a change in temperature and in the chain length. These simulations have been important since no experimental results of the solubility of water in polyethylene at elevated temperatures are available (the necessity to use high temperatures for polyethylene simulations is described later). The reason for this is that the method to measure the low solubility of water in polyethylene is gravimetry, and there is an increasing tendency for water to condens on the surface of the sample as the temperature approaches the critical temperature (of water). Results of the mutual solubilities of water and n-alkanes are more common, both since it is easier to measure and because of its great importance for the petroleum industry.

The classical usage of the Gibbs ensemble method is for the simulation of vapour–liquid equilibria in one or two component systems. Systems consisting of two or more components can have more than two stable phases (e.g. liquid-liquid-vapour equilibrium), and the Gibbs ensemble simulation should have as many boxes as the number of possible phases. The simulations of more than two phases becomes very complex and time consuming, and have not been performed on systems containing more than three phases (three boxes). Another way to overcome the problem is to set up the simulation conditions in such a way that a two phase system is ensured. In the case of water and n-alkanes can this be achieved by performing the simulation at a pressure that is high enough to ensure that the vapour phase dissapears, the remaining two phases are both in the liquid state. It is possible to do this since the mutual solubilities of water and n-alkanes are not very sensitive to variations in pressure. The system pressure must be set higher than the highest vapour pressure of the two components at the temperature studied. It is in most systems in this study water that has the highest vapour pressure, e.g. the water vapour pressure at 450 K is approximately 10 bar. The exeption is hexane which has a vapour pressure of 12 bar (at 450 K), where the corresponding value for octane is 3 bar and the vapour pressures of n-alkanes decrease rapidly with increasing

chain length.

The previously described pure water simulations have been performed in the NVT ensemble, where the number of molecules (N), system volume (V) and temperature (T) are fixed, the system pressure is an output from the simulation. This method is not feasible for liquid – liquid simulations, where the total volume of the system is determined by the number of molecules and the density of each phase. For a liquid–liquid system the NPT ensemble, where the number of molecules (N), the system pressure (P) and the temperature (T) are fixed, is more suitable. In this ensemble, the total system volume is adjusted to provide for the equilibrium densities of the two phases during the simulation.

The acceptance ratio for a particle swap becomes low, since the simulation is between two dense phases and hence the probability that an attempted insertion is made to a part of the simulation box where there is free volume is low. The simulation runs must therefore be very long, and this is probably the reason why only a few Gibbs ensemble studies of liquid–liquid equilibria have been performed.

The most commonly used alkane forcefields are based on the united atom concept, which, in the case of alkanes, means that a carbon atom and the hydrogens bound to it are treated as one single bead. A model without this simplification would require many times longer simulation times, since the system would contain more than three times more beads (three hydrogens on an end carbon and two on the others in the case of n-alkanes) if the hydrogens were treated explicitly. Another common simplification that saves computational time is that the bond length between the united atoms has a fixed value. The models have an equilibrium bond angle (involving three united atoms) with a corresponding bond bending potential, and an equilibrium torsional angle (for atoms separated by two atoms, with an axis through these two atoms), with a corresponding torsional potential. Intermolecular interactions between atoms separated by three or more atoms are calculated using the common Lennard–Jones potential (Equation 1).

Since there are an infinite number of different conformations of an alkane molecule, propane and longer (described using the simplifications described below), the Monte Carlo moves previously described in the water section are not sufficient. The Configurational Bias method[36] (CBMC) has been developed to allow for the efficient simulation of long chain molecules. In this method beads at the end of a chain are deleted, where the number of beads is randomly chosen, and the chain is

then rebuilt bead by bead to form a new conformation. This method is very efficient to simulate alkane molecules with a length up to C_{30} (Ref 37). Other methods for simulating chain molecules (which have not been used in the simulations described in this section) are described in connection to polymer simulations.

There have only been few molecular simulation studies of solubilities of water in hydrocarbons. Gibbs ensemble studies of water-methane and water-ethane mixtures have been performed by Errington et al.[38] Their simulated water-in-alkane and alkane-in-water solubilities, which have involved the SPC/E and TraPPE[39] (alkane) force fields, are in good agreement with experiment. This group has also used the Widom insertion method to study the solubility of water in butane and hexane[40]. Their simulations, which were based on the EP-6 models of water[16] and alkane[41], underestimated the water solubility. The property obtained using the Widom method is the Henry's law constant. Unfortunately, there is no structural information obtained about the solute, or if it affects the structure of the solvent.

To obtain a force field that provided good solubility data at different temperatures (350 – 550 K) and chain lengths (C_6 – C_{16}) using the same set of parameters, different models of water and alkanes were evaluated. The experimental solubility data for C_6 to C_{16} at 450 K and for C_{10} at different temperatures were taken from Economou and Tsonopoulos[42,43]. To account for water solubility in hydrocarbons with longer chains, data[44] calculated with the Sanchez-Lacombe equation of state[45,46] were used for C_{36} and C_{142}. Linear regression fit of the water solubilities in mol% (χ) vs chainlength (n) in alkanes (C_6 – C_{142}) at 450 K gives the expression;

Equation 5:

$$\chi = 5.8422 + 0.068525n$$

and the simulated solubility data at different chainlengths were fit to this expression rather than the experimentally obtained data.

Initial simulations were performed by combining the SPC/E and TraPPE models. This set has previously, as mentioned, been successfully used for water-methane and water-ethane mixtures. An advantage of using SPC/E would be that the water structure could be directly compared to pure water vapour, studied in Paper II. To calculate the Lennard–Jones interactions between different

atom types Lorentz-Berthelot mixing rules[47] were used. In these mixing rules the Lennard-Jones diameter (σ) between species *i* and *j* is calculated with;

Equation 6:

$$\sigma_{ij} = \tfrac{1}{2}(\sigma_i + \sigma_j)$$

and the Lennard–Jones energy parameter, ε, is estimated from;

Equation 7:

$$\varepsilon_{ij} = (\varepsilon_i \varepsilon_j)^{1/2}$$

Unfortunately the water solubility in the hydrocarbons were only approximately one fourth of experimental values. Alkane solubilities in water were low, similarly to experiment. Replacing SPC/E water with SPC increased water-in-alkane solubilities to approximately half of experimental values, but the alkane-in-water solubilities increased by one order of magnitude.

Another alkane model, presented by Karayannis et al.[48,49], was also tested. This model reproduces polyethylene properties very well, but it was not possible to use the model for short alkanes. The interaction energy parameters for this model are too weak when used for short chains, e.g. the density of liquid hexane was only 10% of the experimental value. The potentials for the two hydrocarbon models are shown in Table 1.

To improve the solubility results a parameter that modified the Lennard–Jones energy parameter (ε) was introduced;

Equation 8:

$$\varepsilon_{ij} = B(\varepsilon_i \varepsilon_j)^{1/2}$$

This modified version of the Lorentz-Berthelot mixing rules were only used for interactions between water and alkanes. Intermolecular interactions between water and inter- and intra-molecular interactions between alkanes were calculated using unmodified Lorentz-Berthelot mixing rules.

The best fit for water-in-alkane solubilities were obtained with the parameter B=1.30 for systems of SPC and TraPPE. Since the parameter fit was done in increments of 0.10 it is possible that the results can be further improved using smaller increments of the B parameter.

Unfortunately it was not only the water-in-alkane solubilities that increased, but the alkane-in-water solubilities also increased considerably. This indicates that it is very difficult to find a simple description of water – hydrocarbon interactions that reproduces the mutual solubilities accurately.

The results in terms of densities and solubilities of different models and different B parameters are shown in Table 2.

POLYMER SIMULATIONS

APPENDED PAPER IV

The previously described water-alkane simulations were performed since there are only very few solubility data on polyethylene at high temperature[44] and no experimental data are available to confirm the calculated results. It was thus necessary to develop model parameters on shorter hydrocarbons, but the primary goal has been to simulate polyethylene systems. Two different sytems including polyethylene have been simulated, one small system consiting of five chains with an average length of 100 carbon units [thus consisting of 500 (united) atoms] and one large which contains 10 chains with an average length of 300 carbon units (total of 3000 atoms). The density of amorphous polyethylene is strongly coupled to the chain length as long as the number of carbon units per chain are less than ≈200, whereas the density increases only slowly as function of carbon units when chains are longer[48].

The lowest energy conformation of a polyethylene chain at lower temperatures is planar zig-zag, hence can the chains easily pack into crystals, but different mechanisms restricts the the formation of a perfectly crystalline material, e.g. due to entanglements of the polyethylene molecules. Hence polyethylene is a semicrystalline polymer at temperatures below its melting temperature of ≈415 K (the exact equilibrium melting temperature is a function of chainlength and crystal thickness), at higher temperatures the whole material (the melt) is amorphous due to entropic effects. The polymer can consist of up to, and over, 95 mass % crystalline material[50,51], even if a lower degree of crystallinity is the more common case. Polyethylene with very high degree of crystallinity is very brittle. A reason that the amorphous portion is present, except for the previously mentioned entanglements, is the crystallization mechanism, where crystals grow from different crystallization sites upon cooling from the molten state. The radius of gyration of a chain does not change during

the crystallization, the chain is folded locally, forming crystals together with other chains. Since the molecular packing in the crystals is higher than in the melt, less dense (amorphous) regions must hence be formed outside of the crystals. A spherulite grows radially from a nucleation site, often an impurity, forming crystalline lamellae with a thickness in the region of 10 nm (100 Å). As mentioned, these lamellae are surrounded by amorphous regions, which can have a thickness from less than 10 Å in material with a very high degree of crystallinity, up to 200 Å in material with a degree of crystallinity around 40% (Ref 51). Amorphous regions may also appear when the spherulite has grown large enough to encounter its neighbours, phase separation with respect to e.g. molecular weight may occur during the crystallite growth and different crystallites can normally not join to form larger crystals. Hence amorphous regions are formed around the spherulites. Phase separated (amorphous) regions may also be found inside the spherulite.
No solubility of other molecules is expected in the crystalline parts, with the possible exception of helium (Ref 51). It is thus the amorphous regions that are of interest to study with respect to water solubility. The amorphous region can be considered to consist of different phases, a fully amorphous, liquid-like part far away from the crystalline material and another, intermediate, phase closer to the crystalline surface. The mobility of penetrants is expected to be highest in the intermediate phase, where the mobility of the polymer molecule segments is restricted since most of the polymer molecules in the amorphous phase also form part of the crystalline phase, and are thus constrained where they spring out of the crystal. Typical values for the mass fraction of the different amorphous phases in linear polyethylene with a degree of crystallinity of ≈72% are 14% of the intermediate phase and 14% of the fully amorphous phase, where the average thickness of the amorphous phases were 8.6 Å (Ref 51). It can be expected that the thickness of the fully amorphous phase is half of that value since half of the amorphous portion consists of the fully amorphous phase.
The fraction of the fully amorphous phase is larger in branched polyethylene.

It would, unfortunately, be difficult to simulate this intermediate phase with commonly used molecular simulation methods since the material is anisotropic in these regions. Periodic boundary conditions can therefore not be used, and it would hence require the use of an enormous simulation box to minimize surface effects, which is not feasible due to restrictions in computational capacity.

The cubic polymer simulation box of the large system has a side length of approximately 45 Å. This

is close to the width of the fully amorphous phase in the previous example. It can thus be expected that the system size can represent this phase where the segmental mobility is not significantly affected by the surrounding crystalline parts.

It should be noted that today's high voltage cable insulation is made of crosslinked polyethylene (XLPE) where the whole material can be considered as one single giant molecule. The crosslinking reduces the segmental mobility, but since XLPE contains both crystalline and amorphous parts the molecular scale properties can be considered to be quite similar for XLPE as for the linear polyethylene used in this study. The reason that XLPE has replaced ordinary polyethylene for high voltage insulation purposes is since XLPE, with its higher mechanical strength, has a considerably higher breakdown field strength.

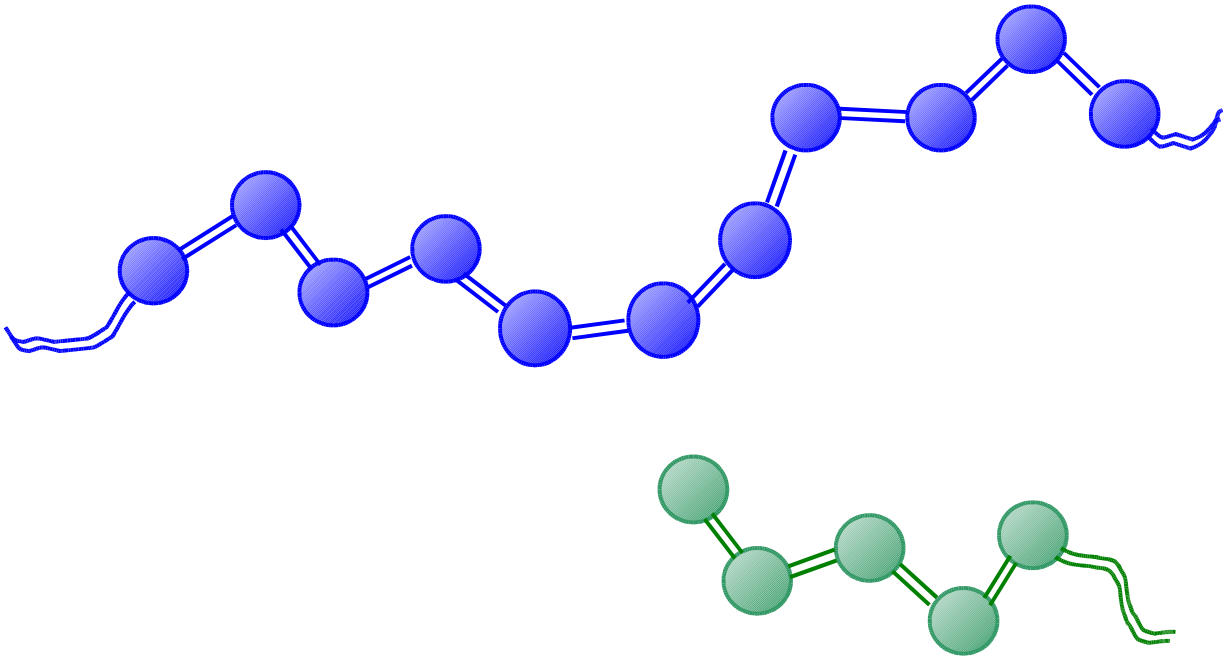

Figure 8: End-bridging Monte Carlo. Two chains on which an end-bridging attempt will be made.
(Published with permission from D. Theodorou, National Technical University of Athens.)

The Monte Carlo moves used for the polymer simulation are reptation, end mer rotation, monomer flip, dimer flip and end-bridge. Fluctuations of the box volume were also allowed. In the reptation move an atom (united atom) is deleted in one end of a polymer chain, the atom is then placed at the other end of the chain. End mer rotation is, as the name suggests, a rotation of the end atom around the axis formed by the second and third atom from the end. The monomer flip move means

that an atom in the chain is rotated around the axis formed by its two neighbours in the chain and dimer flip is a similar move, but where a group of two neighbouring atoms is rotated.

The most important of the Monte Carlo moves used in the polymer simulations is end-bridging[52]. As illustrated in Figures 8 and 9, in this move atoms belonging to one chain can alter connectivity and join to the end of another chain. The donor chain thus shortens by the same number of beads as the second chain accepts. This is achieved by constructing a trimer between the end atom of one chain and a selected interior atom on another chain from which the attempt to remove atoms is made. The distance between these two atoms must be shorter than the distance that the four bonds, with fixed equilibrium angles, that are involved in a trimer that forms an interior part of a longer chain can bridge. If this criterion is fullfilled there are always geometric solutions to the the trimer bridging problem, and these solutions can be found numerically. If the move is accepted a trimer in the donor chain is deleted, and the number of atoms in the system are thus kept constant.

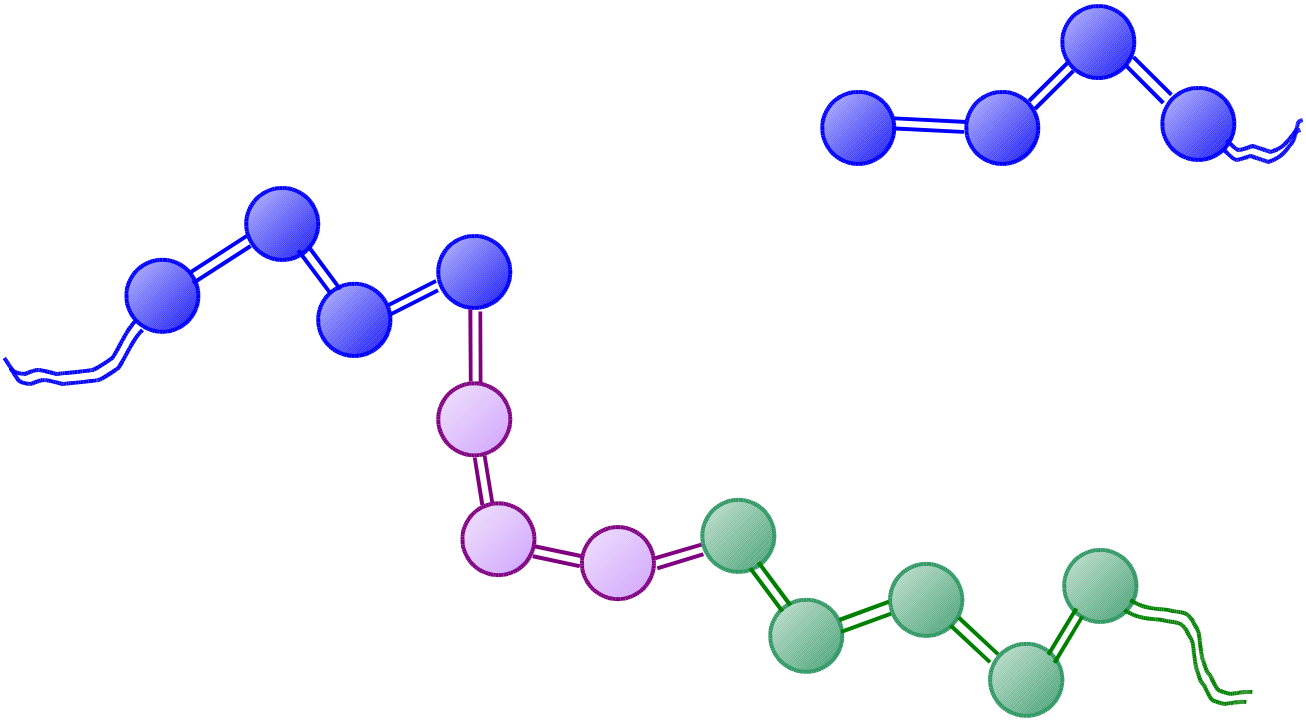

Figure 9: End-bridging Monte Carlo. A trimer has successfully been constructed and the left part of the blue chain has been connected to the green chain.
(Published with permission from D. Theodorou, National Technical University of Athens.)

It is obvious that the lengths of the chains are altered when using this move, and it is thus not possible to maintain a monodisperse system. In order to keep the number of chains in the system constant the length of the chains must be restricted, with both a maximum and a minimum length. The average chain length is in the middle of this interval. The larger the interval between shortest and longest allowed chain length, the larger is the probability that the move is accepted since there is a larger possibility that a chain end is close enough to another chain on which an attempt to do the move is allowed. In the work presented here the longest allowed chain length has been 50% longer than the average chain length, the shortest allowed chain length was thus half of the average length. Even with this large degree of polydispersity, most of the attempted end-bridging moves are rejected, and only 0.3% were accepted. This value is not affected by the chain length, it is the same for both the large and the small systems. This acceptance ratio can be compared to 8% accepted reptation moves, 18% accepted end mer rotation, 67% accepted dimer flip and 78% accepted monomer flip. It can seem that such low acceptance ratio for end-bridging moves would indicate that the move is inefficient, but it is the fastest existing method for Monte Carlo simulations of polymers. To equilibrate a polymer system using configurational bias would take many orders of magnitude longer computational time[37].

Entanglements cannot restrict the segmental moves when connectivity-altering methods are used, the entanglements will eventually be untied if the simulation is long enough. That means that the equilibrated system will take its lowest energy configuration, which is the fully crystalline if the temperature is lower than the melting temperature. It has thus been necessary to perfom the simulations at a higher temperature. A temperature of 450 K has been chosen, since this is considerably higher than the melting temperature of real polyethylene. The melting temperature of TraPPE polyethylene is not known, but it is clear that it is in the molten state at 450 K. This temperature has also been used in most studies of polyethylene using connectivity-altering methods with TraPPE and other polymer models[37,48,49].

To study polymers at technically relevant temperatures for cable insulation purposes (up to 350 K) would require other simulation methods, e.g. molecular dynamics simulations on systems where the polymer melt have been equilibrated using Monte Carlo methods at higher temperatures. Unfortunately, molecular dynamics does not allow insertions of water molecules, which is an unphysical event, when Newton's equation is used. The composition of the system must be fixed to an experimentally obtained water solubility (as mentioned these results are scarce), and it is thus not known if the simulation is performed on a system with equilibrium composition.

EXTERNAL ELECTRIC FIELDS

APPENDED PAPER V

The total potential energy (U) in a system with an external electric field (**E**) is:

Equation 9:

$$U = U_0 - \mathbf{M} \bullet \mathbf{E}$$

where U_0 is the potential energy in the absence of an external field and **M** is the sum of the molecular dipole moments. The energy contribution from the external field is a scalar. The equation in the appended Paper V is unfortunately a bit ambigious since the multiplication sign has been expressed with a cross, which can be misinterpreted as refering to a vector product.

The external field has been applied in one direction, parallel to the X axis. In practice the calculation of the energy contribution from the external field is achieved by multiplying the charge (in the unit e) with the field and with the X coordinate (unit Å) of the charge. The coordinate dependence on the energy of the charges, which gets larger when the X coordinate increases, disappears since the net charge of each water molecule is zero. The positive contribution from the hydrogen coordinates and the negative contribution of the oxygen cancels out and only the contribution that stems from the molecules orientation in the field remains. The unit of the field is K/(e*Å), which can be converted to V/m by using the following conversion factor;

Equation 10:

$$1 \text{ V/m} = 1.1604 * 10^{-6} \text{ K/}(e*\text{Å})$$

where 1 K corresponds to $1.38 * 10^{-23}$ J which is known as Boltzmann's constant, k_B.

The external electric field has only been implemented in the polymer simulation program, and simulations have only been performed on the large polyethylene system. No data on water solubilities in n-alkanes exposed to external electric fields are published, and it was hence no advantage of simulating these systems as reference (except for the effect of varying the temperatures).

It is only the water that is directly affected by the electric field, since TraPPE polyethylene is non-polar and has no charges. It is possible that that the results at the highest fields would be affected if a polyethylene model with explicit hydrogens (and implemented partial charges) were used. But such a simulation study would be difficult using todays computers since, as previously mentioned, it would include four times more Lennard–Jones sites, and approximately hundred times more charged sites. It can thus be expected that such a simulation would take two to three orders of magnitude longer time.

The same can be said about the water model, since field induced polarization may affect the water at the highest fields, but the trends are expected to be the same since the effect of the fields on the water solubility in polyethylene and liquid water density is seen already at fields that are only 10% of the local field between two water molecules. The liquid structure has not been studied by means of rdf's or orientational analysis, but it is has been seen that the liquid water orients in the direction of the field at external fields much lower than the local field between water molecules by visual checks of the liquid water box. These visual checks do not show any preferential direction of the water molecules at a field of 6×10^7 V/m. At a field of 2×10^8 V/m is it clear that the molecules are beginning to orient in the field, at 9×10^8 V/m there are only few water hydrogens that are directed against the field and most of the molecules are strongly directed in the field at 4×10^9 V/m, even though they don't show the highly ordered crystalline structure found when the external field is ten times higher[53].

The effects on the rdf's of an external field on a large water cluster have been studied in the appended Manuscript VII though, and there can it be seen both that the field decreases the intermolecular distance and that the molecules are more oriented in a high field. It is probably a combination of these two effects that lies behind the rapidly increased liquid density at the highest fields.

SIMULATION OF IONS, WATER AND HYDROCARBONS

ROD-LIKE WATER CLUSTER SIMULATIONS

APPENDED MANUSCRIPT VI

It is clear from the previous discussion and Paper V that water in polyethylene exposed to high external electric fields does not tend to form large clusters, and thus that it could be expected that

the field alone cannot initiate water tree growth. This is also supported by the fact that it is very difficult to grow water trees if the sample is immersed in pure water instead of water containing ions[4].

Different ions are always present in the environment, and it is inevitable that a high voltage cable comes into contact with them. Impurities are also present in real polyethylene. These impurities can have several origins that stem from the production of the polymer and from the processing of the material when cables are produced[54]. One is in the form of peroxides, added for the crosslinking of XLPE, and there will always be residues left in the material. Other sources of contamination from the polymer production are metal particles originating from the reactor and pipes, and oil from pumps. Sources from the manufacturing of cables are carbon black used in the semiconductive layer surrounding the conductor, copper particles from the conductor and iron particles from the extruder. A large part of these particles are large on a molecular scale, and are thus essentially immobile in the polymer matrix.

To model the contamitants one positive ion (Na^+) and one negative ion (Cl^-) have been used in the systems. The Dang models[55] were chosen to represent the ions. These models have a Lennard–Jones potential (see Table 1) and a charge of +1 *e* (Na^+) and -1 *e* for (Cl^-). The Dang models have been developed to be used together with SPC/E water, and hence this water model has been used in the simulations. Since the bulk solubilities of water in the hydrocarbon is not the main interest in this study the Lorentz–Berthelot mixing rules have been used, without the fitting parameter used for ε in the previous studies. As previously mentioned, the SPC/E water solubilities in hydrocarbons are only one fourth of the experimental values. Since the solubility results from this study are not directly comparable to the previous results, the solubilities from this study are a function of ion concentration on a larger scale. The lower solubility of SPC/E water in hydrocarbon only emphasizes the effect of the ions.

The two oppositely charged ions were fixed at relative positions in the hydrocarbon box, with initial distances of 15, 20 or 25 Å. There was no water in the hydrocarbon box when the simulations started. Since the box size increased when water was absorbed, the ion distances for equilibrated decane systems increased by approximately 0.3 Å. The ion distance in the polyethylene system increased from 20 to 20.05 Å. The fixed ion positions is not an equilibrium condition, and it could be expected that the ions would slowly approach each other until they reach a shorter equilibrium

distance if they were allowed to move. A decreasing ion distance has also been observed in a simulation where translations were applied also to the ions. Even if it is not true equilibrium conditions, the fixed ion distance allows for a systematic study of the effect of ions under different conditions, and since Monte Carlo simulations do not involve time will it show the equilibrium structure when the ions are separated by the distance used. The ion distances correspond to the average distances between ions in aqueous solutions with ion concentrations of 0.5 M (15 Å), 0.2 M (20 Å) and 0.1 M (25 Å). The ion concentration of the salt water used in experiments on water tree initiation and growth is in the region of 0.05 – 0.1 M (Ref 4), and since the water absorption, and hence ion absorption, is relatively low, the average ion separation will be larger than the distances used in this study. But, since ions cannot be expected to be evenly distributed in the polymer matrix, and since there are an enormous amount of ions present, there will be a lot of ions pairs separated by the distances used in the simulations.

The results show that it is not necessary to study systems with larger ion separations than what have been used in the study. Longer ion separations are also difficult to achieve, due to the periodic boundary conditions. An ion distance of 20 Å in the X direction in the polymer box (side length 45 Å) is straightforward, but the decane box has a side length of less than 35 Å, and there it was necessary to place the ions diagonally in the box in order to achieve the larger ion separations and still be sure that the distance to the six replicas in the surrounding boxes are larger than the distance that was intended to study in the system.

The energy (u) between two charges in the unit K is:

Equation 11:

$$u = (q_1 q_2 / r^2)* \mathrm{k}$$

where r is the separation in Å, q is the charge in e and

Equation 12:

$$\mathrm{k} = e^2 * 10^{10} /(4\pi\varepsilon_0 k_B)$$

where ε_0 is the permittivity in vacuum (in As/Vm). If a particle, in this case a hydrogen or oxygen

in a water molecule, is influenced by two charged particles the total potential energy is the sum of the interactions between the particle and each of the two charged species. In a one-dimensional example where the water molecule is simplified to a dipole, located a certain distance from the negative ion on the axis passing through the two ions, with the postive charge closer than the negative to the negative ion, is the energy lower if the dipole is located between the ions than if the dipole is located outside (and where the dipole is reversed) the negative ion. It is thus energetically more favourable for the water molecules to be located between the ions than outside the region between the ions. This is reflected by the large cluster with rod-like water formed between the ions. It is also a fact that the solubility of water molecules far away from the cluster formed between the ions is much lower than in the previously studied systems in the absence of ions, but this is probably since the water solubilities are lower with the model parameters used in this study than in the systems previously studied.

The electric field between two oppositely charged particles is lowest midway between the particles (on an axis passing through the particles), and the lowest field strength between the bare Na^+ and Cl^- ions separated by 15 Å is 5.1×10^9 V/m, when separated 20 Å it is 2.8×10^9 V/m and 1.8×10^9 V/m when the ion separation is 25 Å. This can be compared to $\approx2\times10^9$ V/m that corresponds to a typical hydrogen bond energy between two SPC/E water molecules. It seems that the large cluster formed between the ions cannot be maintained when it is not supported by a field that is larger than the local field between the water molecules, at least not at the relatively high temperature of 400 K.

The fluctuations in all of the properties investigated in Manuscript VI are much slower in the polyethylene simulations, due to its higher density and cohesive energy, than in the decane simulations. Thus the polyethylene simulations must be longer. This has motivated that most of the study has been performed on decane, together with the opportunity to study temperature effects on decane systems. Two other effects that restrict the fluctuations are illustrated in Figure 10, where the number of configurations with a certain number of water molecules in the decane box is plotted. As expected, the thermal fluctuations – or width of the distribution – increases with increasing temperature. The number of molecules in the systems where the ion distance is 15 and 25 Å is in both cases lower than when the separation is 20 Å, in the first case since the cluster is smaller and in the latter case since there are two small clusters instead of one large. The narrower distrbution at the smallest ion separation is due to that the higher field between the ions is restricting the fluctuations.

Figure 10 also gives an indication of the size of the cluster between the ions, since at least 97 % of the water molecules in the box is included in the physical cluster (the two clusters for 400 K with 25 Å ion separation) between the ions. It can be noted that interactions with the surrounding hydrocarbon are restricting the size of the cluster. A Gibbs ensemble simulation of water (in the absence of hydrocarbon) with the two ions fixed at a distance of 20 Å at 450 K renders an average vapour cluster size around 50 water molecules.

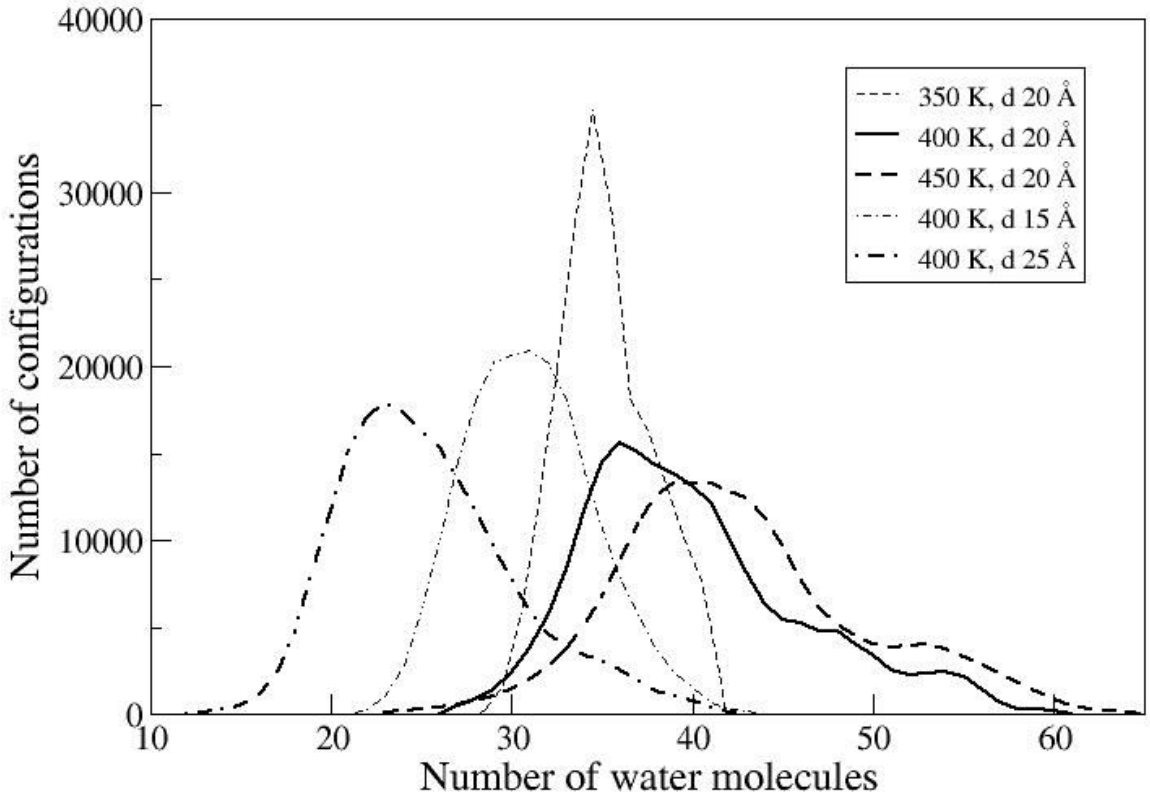

Figure 10: Distribution of configurations containing a given number of water molecules in decane, as a function of temperature and Na^+--Cl^- distance. The total number of configurations is 200 000.

ROD-LIKE WATER IN EXTERNAL ELECTRIC FIELDS

APPENDED MANUSCRIPT VII.

All methods used in this study have been described previously. This study differs from the study in the appended Manuscript VI in that an external field has been applied, and in that it has only been performed on polyethylene (C_{300}).

The acceptance ratio of swap moves decreases rapidly when the field is increased. This increases the statistical uncertainity of our results and it is thus only possible to assume a trend that the water cluster size increases with increasing external field. This decreased mobility at higher external fields is illustrated in Figure 11, where the distribution of the number of water molecules in the physical cluster formed between the ions is shown. Note that the data are taken from a simulation period that is less than 10% of the total simulation. The reason do to this is described below. Thus, the average cluster sizes are not exactly corresponding to the average number of water molecules in the polymer box shown in Figure 1 in Manuscript VII. Figure 11 shows that the fluctuations during the short simulations gets smaller when the field is increasing, and based on an analysis of the number of water molecules in the polymer phase from simulations of different lenghts, there is a need for very long simulations in order to be sufficiently long to allow sampling of the relevant configurational space. Other properties than the cluster size that are discussed in this study are not affected by these slow fluctuations. The trend with the narrower cluster size distribution in the highest field was also seen with ions in decane at 400 K with a separation of 15 Å (Figure 10), where the local field between the ions is higher than when the ion distance is larger. Cluster analysis has only been performed on a fraction of the simulation lengths since the cluster analysis is very time consuming for these large clusters and the cluster size distributions presented in Figure 11 took on average four weeks to perform (with the cluster analysis program available, which is not optimized for the study of large clusters).

The critical cluster size of the water cluster between the polymer-bound ions is mentioned in the manuscript. The critical cluster size of a water cluster in polyethylene at 450 K exposed to an external electric field is not known, but it is clearly larger than the cluster sizes found in this study. Most of the studies of critical cluster growth in vapour have been performed at temperatures below 300 K, but there exists a molecular dynamics study[56] of TIP4P water at 350 K where the critical cluster size was estimated to be 30 – 45 vapour water molecules. Critical cluster size increases with increasing temperature, and the average vapour water cluster size of 50 molecules at 450 K reported in the previous section is not sufficiently large to cause critical cluster growth. Another variable is that the critical cluster size is decreased considerably in the presence of an external electric field[57] (by over 30 % in a field 10^9 V/m).

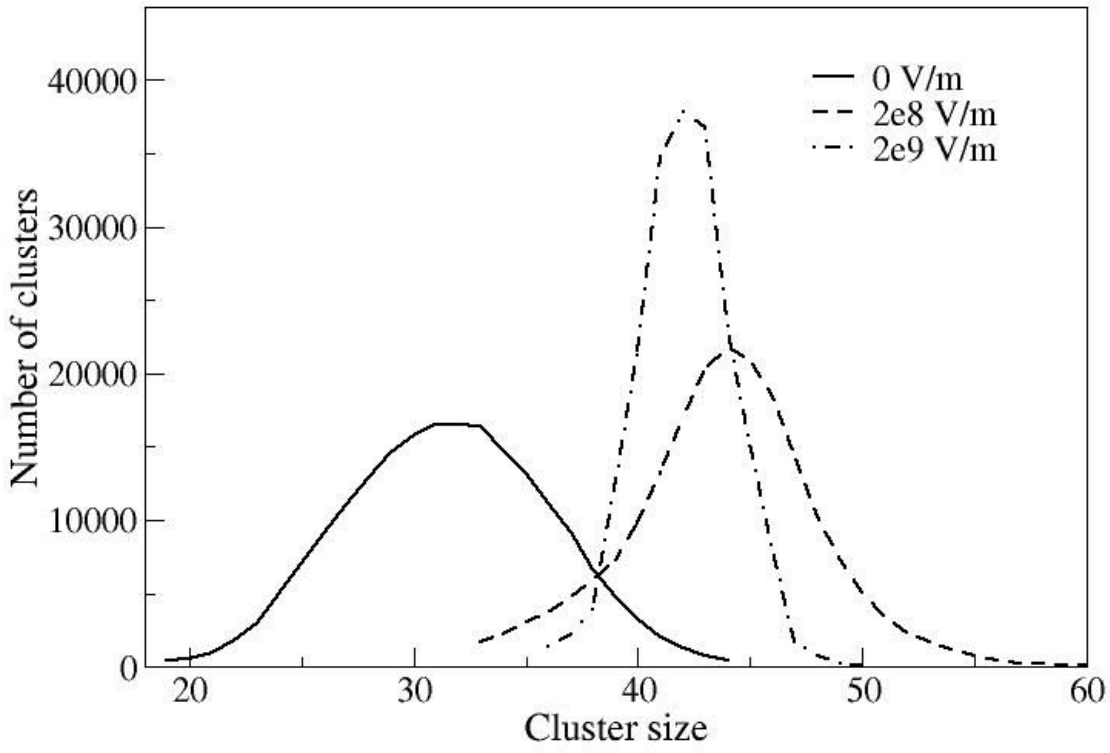

Figure 11: Distribution of water cluster sizes in polyethylene systems exposed to different external electric fields at 450 K. The total number of clusters is 200 000 for each system.

REFERENCES

[1]P. Chýlek, Q. Fu, H. C. W. Tso and D. J. W. Geldart, Tellus **51A**, 304 (1999).

[2]M. Fukuda, J. Chem. Phys. **109**, 6476 (1998).

[3]T. Tabata, T. Fukuda and Z. Iwata, IEEE Trans. PAS-91, 1361 (1972).

[4]A. T. Bulinski, J.-P. Crine, B. Noirhomme, R. J. Densley and S. Bamji, IEEE Trans. Dielectr. Electr. Insul. **5**, 4 (1998).

[5]L. A. Dissado and J. C. Fothergill, *Electrical degradation and breakdown in polymers* (Peter Peregrinus Ltd, London, 1992).

[6]Patsch R, IEEE Trans. Electr. Insul., **27**, 3 (1992).

[7]I. Radu, M. Acedo, J. C. Fillippini, P. Notingher and F. Frutos, IEEE Trans. Dielectr. Electr. Insul. **7**, 860 (2000).

[8]J. Sletbak, *Proc 3rd ICPADM*, Tokyo, 208 (1991).

[9]J. P. Jones, J. P. Llewellyn and T.J. Lewis, IEEE Trans. Dielectr. Electr. Insul. **12**, 951 (2005).

[10]A. Z. Panagiotopoulos, Mol. Phys. **61**, 813 (1987).

[11]H. J. C. Berendsen, J. R. Grigera and T. P. Straatsma, J. Phys. Chem. **91**, 6269 (1987).

[12]Frenkel and B. Smit, *Understanding Molecular Simulation from Algorithms to Applications* , 2nd ed. (Academic, New York, 2002).

[13]P. P. Ewald, Ann. Phys. **64** (1921).

[14]G. C. Boulougouris, I. G. Economou and D. N. Theodorou, J. Phys. Chem. B **102** ,1029 (1998).

[15]H. J. C. Berendsen, J. P. M. Postma and W. F. van Gunsteren, in *Intermolecular Forces,* edited by B. Pullman (Reidel, Dordrecht, 1981) p. 331.

[16]J. R. Errington and A. Z. Panagiotopoulos, J. Phys. Chem. B **102**, 7470 (1999).

[17]I. G. Economou, Fluid Phase Equilib. **183-184**, 259 (2001).

[18]P. Mark and L. Nilsson, J. Phys. Chem. A **105**, 9954 (2001).

[19]W. L. Jorgensen, J. Chandrasekhar J. D. Madura, R. W. Impey and M. L. Klein, J. Chem. Phys. **79**, 926 (1983).

[20]C. Peltz, A. Baranyai, A. A. Chivalo and P. T. Cummings, Molecular Simulation **29**, 13 (2003).

[21]M. W. Mahoney and W. L. Jorgensen, J. Chem. Phys. **112**, 8910 (2000).

[22]L. M. Svishchev, P. G. Kusalik, J. Wang and R. J. Boyd, J. Chem. Phys. **105**, 4742 (1996).

[23]T. M. Hayward and I. M. Svishchev, Fluid Phase Equilib. **182**, 65 (2001).

[24]M. Lísal, W. R. Smith and I. Nezbeda, Fluid Phase Equilib. **181**, 127 (2001).

[25]S. W. Rick, J. Chem. Phys. **120**, 6085 (2004).

[26]M. Lísal, I. Nezbeda and W. R. Smith, J. Phys. Chem. B **108**, 7412 (2004).

[27]D. van der Spoel, P. J. Van Maaren and H. J. C. Berendsen, J. Chem. Phys. **108**, 10220 (1998).

[28]P. M. King, Mol. Phys. **94**, 717 (1998).

[29]P. Jedlovszky and J. Richardi, J. Chem. Phys. **110**, 8019 (1999).

[30]F. H. Stillinger, J. Chem. Phys. **38**, 1486 (1963).

[31]A. G. Kalinichev and J. D. Bass, J. Phys. Chem. A **101**, 9720 (1997).

[32]J. Qian, E. Stöckelmann and R. Hentschke, J. Mol. Model. **5**, 281 (1999).

[33]B. Chen, J. J. Potoff and J. I. Siepmann, J. Phys. Chem. B **104**, 10 (2000).

[34]http//kea.princeton.edu/jerring/gibbs/index.html.

[35]D. N. Theodorou and U. W. Suter, J. Chem. Phys. **82**, 2 (1985).

[36]J. I. Siepmann and D. Frenkel, Mol. Phys.**75**, 59 (1992).

[37]V. G. Mavrantzas, T. D. Boone, E. Zervopoulou and D. N. Theodorou, Macromolecules **32**, 5072 (1999).

[38]J. R. Errington, G. C. Boulougouris, I. G. Economou, A. Z. Panagiotopoulos and D. N.

Theodorou, J. Phys. Chem. B **102**, 8865 (1998).

[39]M. C. Martin and J. I. Siepmann, J. Phys. Chem. B **102**, 2659 (1998).

[40]G. C. Boulougouris, J. R. Errington, I. G. Economou, A. Z. Panagiotopoulos and D. N. Theodorou, J. Phys. Chem. B **104**, 4958 (2000).

[41]J. R. Errington and A. Z. Panagiotopoulos, J. Phys. Chem. B **103**, 6314 (1999).

[42]I. G. Economou and C. Tsonopoulos, Chem. Eng. Sci. **52**, 511 (1997).

[43]C. Tsonopoulos, Fluid Phase Equilib. **156**, 21 (1999).

[44]C. W. Haschets, A. D. Shine and R. M. Secor, Ind. Eng. Chem. Res. **33**, 1040 (1994).

[45]I. C. Sanchez and R. H. Lacombe, J. Phys. Chem. **80**, 2352 (1976).

[46]I. C. Sanchez and R. H. Lacombe, Macromolecules **11**, 1145 (1978).

[47]H. A. Lorentz, Ann. Phys. **12**, 127 (1881), D. C. R. Berthelot, Hebd. Seances Acad. Sci. **126**, 1703 (1898).

[48]N. C. Karayannis, V. G. Mavrantzas and D. N. Theodorou, Phys. Rev. Lett. **88**, 10 (2002).

[49]N. C. Karayannis, A. E. Giannousaki, V. G. Mavrantzas and D. N. Theodorou, J. Chem. Phys. **117**, 11 (2002).

[50]U. W. Gedde, *Polymer physics* (Kluwer Academic Publishers, Dordrecht, 1999).

[51]M. Hedenqvist, A. Angelstok, L. Edsberg, P. T. Larsson and U. W. Gedde, Polymer, **37**, 8 (1995).

[52]P. V. K. Pant and D. N. Theodorou, Macromolecules **28**, 7224 (1995).

[53]G. Sutmann, J. Electroanal. Chem. **450**, 289 (1998).

[54]U. Nilsson, Borealis AB, Stenungsund, Sweden (personal communication).

[55]D. E. Smith and L. X. Dang, J. Chem. Phys. **100**, 3757 (1994).

[56]K. Yasouka and M. Matsumoto, J. Chem. Phys. **109**, 19 (1998).

[57]G. T. Gao, K. J. Oh and X. C. Zeng, J. Chem. Phys. **110**, 2533 (1999).

Table 1. Model potentials

	Bond lengths	Nonbonded interactions $V_{LJ}(r_{ij}) = 4\,\epsilon_{ij}\left[\left(\frac{\sigma_{ij}}{r_{ij}}\right)^{12} - \left(\frac{\sigma_{ij}}{r_{ij}}\right)^{6}\right]$	Bond bending $\frac{V_{bend}(\theta)}{k_B} = \frac{1}{2}k_\theta(\theta - \theta_0)^2$	Torsion angles	Charge
SPC/E water	1.0 Å, fixed	$\frac{\epsilon_O}{k_B} = 78.21\,\mathrm{K}$ σ_O = 3.166 Å	$\theta_0 = 109.5^o$ fixed		q_O = -0.8476e q_H = 0.4238e
SPC water	1.0 Å, fixed	$\frac{\epsilon_O}{k_B} = 78.21\,\mathrm{K}$ σ_O = 3.166 Å	$\theta_0 = 109.5^o$ fixed		q_O= -0.82e q_H = 0.41e
TraPPE hydrocarbon	1.54 Å, fixed	$\frac{\epsilon_{CH_2}}{k_B} = 46$ K $\frac{\epsilon_{CH_3}}{k_B} = 98$ K σ_{CH_2} = 3.95 Å σ_{CH_3} = 3.75 Å	$k_\theta = 62500$ K rad^{-2} $\theta_0 = 114^o$	$\frac{V_{tor}(\phi)}{k_B} = c_1[1+\cos(\phi)] + c_2[1-\cos(2\phi)] + c_3[1+\cos(3\phi)]$ c_1= -335.03K, c_2=68.19K, c_3= -791.32K	
Karayannis hydrocarbon	1.54 Å, fixed	$\frac{\epsilon_{CH_2}}{k_B} = \frac{\epsilon_{CH_3}}{k_B} = 46$ K $\sigma_{CH_2} = \sigma_{CH_3}$ = 3.95 Å	$k_\theta = 62500$ K rad^{-2} $\theta_0 = 114^o$	$\frac{V_{tor}(\phi)}{k_B} = \sum_{i=0}^{N} c_i \cos^i(\phi)$ N = 8 c_0= 1001 K, c_1= 2130 K, c_2= -303 K, c_3= -3612 K, c_4= 2227 K, c_5= 1966 K, c_6 = -4489 K, c_7= -1736 K, c_8= 2817 K	
Dang Na		$\frac{\epsilon_{Na}}{k_B} = 7.4301\,\mathrm{K}$ σ_{Na} = 2.5752 Å			q_{Na} = 1.0e
Dang Cl		$\frac{\epsilon_{Cl}}{k_B} = 59.595\,\mathrm{K}$ σ_{Cl} = 4.480 Å			q_{Cl} = -1.0e

TABLE 2. Simulation results

Pressure is 30 Bar, and systems have 200 water and 100 alkane molecules, when nothing else is stated. L-B means that Lorentz-Berteloth mixing rules is used.

Models	***Epsilon O-C*** ***K***	***T*** ***K***	***Rho Waterbox*** ***kg/m³***	***Rho Alkanebox*** ***kg/m³***	***Solubility of water in alkane*** ***(mol%)***	***Solubility of alkane in water*** ***(mol%)***	***Comments***
Water – Hexane Experiment		450	880	483	0.0585	0.859E-05	Densities are for one component systems
Water – Octane Experiment		450	880	559	0.0676	0.628E-05	Densities are for one component systems
Water – Decane Experiment		350	975	≈686	0.0042	0.94E-09	Densities are for one component systems
Water – Decane Experiment		400	937	≈660	0.0188	0.19E-06	Densities are for one component systems
Water – Decane Experiment		450	880	≈600	0.0602	0.65E-06	Densities are for one component systems
Water – Decane Experiment		500	832	≈550	0.1523	0.31E-05	Densities are for one component systems
Water – Decane Experiment		550	757	≈460	0.326	0.18E-04	Densities are for one component systems
Water – Hexadecane Experiment		450	880	≈650	0.0693	Very low	Densities are for one component systems
Water – C_{36} Sanches-Lacombe		450			≈0.09	Very low	
Water – C_{142} Sanches-Lacombe		450		762	≈0.15	Very low	Density is for one component system
SPC/E–TraPPE Hexane	L-B	450	868.8	503.8	0.1158E-01	0.2433E-04	60 Bar
SPC/E–TraPPE Hexane	L-B	450	877.9	488.9	0.1319E-01	0.1125E-04	
SPC/E–TraPPE Hexane	L-B	450	860.0	467.8	0.1470E-01	0.3498E-04	10 Bar, Risk for vapourisation
SPC/E–TraPPE Hexane	110	450	837.8	471.1	0.4240E-01	0.1889E-01	500 water molecules
SPC/E–TraPPE Hexane	B=1.50	450	853.5	478.0	0.3310E-01	0.6806E-02	500 water molecules
SPC/E–TraPPE Hexane	B=1.68	450	824.4	465.7	0.5161E-01	0.3126E-01	500 water molecules
SPC/E–TraPPE Octane	L-B	450	867.1	570.0	0.1095E-01	0.8876E-07	
SPC/E–TraPPE Octane	110	450	833.6	561.7	0.4140E-01	0.2134E-01	500 water molecules
SPC/E–TraPPE Octane	B=1.50	450	861.0	560.5	0.3076E-01	0.3465E-02	500 water molecules
SPC/E–TraPPE Octane	B=1.68	450	818.7	561.9	0.4817E-01	0.3297E-01	500 water molecules
SPC/E–TraPPE Decane	L-B	350	965.0	694.3	0.2607E-03	0.000	500 water molecules
SPC/E–TraPPE Decane	110	350	954.5	693.3	0.1723E-02	0.1381E-01	500 water molecules
SPC/E–TraPPE Decane	B=1.50	350	967.3	693.8	0.1184E-02	0.000	500 water molecules
SPC/E–TraPPE Decane	B=1.68	350	953.9	693.9	0.2070E-02	0.1381E-01	500 water molecules
SPC/E–TraPPE Decane	L-B	400	921.9	654.1	0.2038E-02	0.000	500 water molecules
SPC/E–TraPPE Decane	110	400	906.0	653.3	0.1223E-01	0.1384E-01	500 water molecules
SPC/E–TraPPE Decane	B=1.50	400	910.0	652.1	0.6894E-02	0.6875E-02	500 water molecules
SPC/E–TraPPE Decane	B=1.68	400	920.2	652.8	0.1239E-01	0.000	500 water molecules
SPC/E–TraPPE Decane	L-B	450	865.4	612.6	0.1088E-01	0.000	
SPC/E–TraPPE Decane	L-B	450	865.4	615.9	0.1013E-01	0.000	500 water molecules
SPC/E–TraPPE Decane	B=1.50	450	851.8	606.1	0.2857E-01	0.5680E-02	500 water molecules
SPC/E–TraPPE Decane	B=1.68	450	866.5	607.0	0.6263E-01	0.2020E-02	500 water molecules
SPC/E–TraPPE Decane	L-B	500	802.1	569.6	0.3986E-01	0.1144E-04	60 Bar
SPC/E–TraPPE Decane	B=1.50	500	786.4	558.2	0.1136	0.4587E-02	60 Bar, 500 water molecules
SPC/E–TraPPE Decane	B=1.68	500	725.1	562.7	0.1892	0.4720E-01	60 Bar, 500 water molecules
SPC/E–TraPPE Decane	110	500	770.3	556.8	0.2283	0.2088E-01	60 Bar, 500 water molecules
SPC/E–TraPPE Decane	L-B	550	734.7	566.2	0.8615E-01	0.6000E-04	200 Bar
SPC/E–TraPPE Decane	110	550	Unstable, 616.0	goes to one 570.1	phase system! 0.4934	0.1257	200 Bar, 500 water molecules
SPC/E–TraPPE Decane	B=1.50	550	706.9	551.0	0.2522	0.1213E-01	200 Bar, 500 water molecules
SPC/E–TraPPE Decane	B=1.68	550	Unstable, 596.7	goes to one 596.5	phase system! 0.8639	0.1665	200 Bar, 500 water molecules
SPC/E–TraPPE Decane	80	450	868.3	607.1	0.1702E-01	0.000	500 water molecules
SPC/E–TraPPE Decane	100	450	863.6	608.0	0.3335E-01	0.4331E-03	500 water molecules
SPC/E–TraPPE Decane	105	450	860.0	606.4	0.5111E-01	0.3257E-02	500 water molecules
SPC/E–TraPPE Decane	110	450	850.0	605.6	0.5779E-01	0.1251E-01	500 water molecules
SPC/E–TraPPE Decane	120	450	855.0	613.7	0.2539	0.1135E-01	500 water molecules
SPC/E–TraPPE Decane	277.828 GROMOS	450	Complete	miscibility	of components		500 water molecules
SPC/E–TraPPE Hexadecane	L-B	450	863.3	676.1	0.1147E-01	0.000	
SPC/E–TraPPE Hexadecane	110	450	867.0	672.4	0.1064	0.1937E-02	500 water molecules
SPC/E–TraPPE Hexadecane	B=1.50	450	863.4	676.5	0.3525E-01	0.000	500 water molecules
SPC/E–TraPPE Hexadecane	B=1.68	450	865.6	670.4	0.6853E-01	0.000	500 water molecules

Models	*Epsilon O-C* *K*	*T* *K*	*Rho Waterbox* *kg/m³*	*Rho Alkanebox* *kg/m³*	*Solubility of water in alkane* *(mol%)*	*Solubility of alkane in water* *(mol%)*	*Comments*
SPC-TraPPE Hexane	L-B	450	811.9	477.3	0.3258E-01	0.1352E-03	
SPC-TraPPE Hexane	B=1.20	450	808.7	457.1	0.4858E-01	0.7766E-03	500 water molecules
SPC-TraPPE Hexane	B=1.30	450	806.7	456.9	0.5616E-01	0.2114E-02	500 water molecules
SPC-TraPPE Hexane	B=1.40	450	795.4	455.1	0.6581E-01	0.6598E-02	500 water molecules
SPC-TraPPE Octane	L-B	450	810.2	568.8	0.2320E-01	0.3579E-04	
SPC-TraPPE Octane	B=1.20	450	807.6	557.2	0.3794E-01	0.1955E-03	500 water molecules
SPC-TraPPE Octane	B=1.30	450	808.7	558.5	0.4664E-01	0.9191E-03	500 water molecules
SPC-TraPPE Octane	B=1.40	450	804.9	557.7	0.6189E-01	0.3374E-02	500 water molecules
SPC-TraPPE Decane	L-B	350	934.8	694.5	0.8467E-03	0.000	500 water molecules
SPC-TraPPE Decane	B=1.20	350	934.4	693.2	0.1506E-02	0.000	500 water molecules
SPC-TraPPE Decane	B=1.30	350	933.9	694.2	0.1832E-02	0.000	500 water molecules
SPC-TraPPE Decane	B=1.40	350	935.2	694.4	0.2752E-02	0.000	500 water molecules
SPC-TraPPE Decane	L-B	400	881.9	654.1	0.5281E-02	0.000	500 water molecules
SPC-TraPPE Decane	B=1.20	400	880.9	651.7	0.8099E-02	0.000	500 water molecules
SPC-TraPPE Decane	B=1.30	400	877.8	653.1	0.1104E-01	0.000	500 water molecules
SPC-TraPPE Decane	B=1.40	400	882.1	653.2	0.1521E-01	0.000	500 water molecules
SPC-TraPPE Decane	L-B	450	806.6	611.2	0.2368E-01	0.7552E-06	
SPC-TraPPE Decane	B=1.20	450	812.3	605.1	0.3661E-01	0.5678E-04	500 water molecules
SPC-TraPPE Decane	B=1.30	450	809.0	604.9	0.4510E-01	0.2968E-03	500 water molecules
SPC-TraPPE Decane	B=1.40	450	810.9	605.2	0.5939E-01	0.6660E-03	500 water molecules
SPC-TraPPE Decane	B=1.50	450	795.3	603.6	0.8664E-01	0.1017E-01	500 water molecules
SPC-TraPPE Decane	L-B	500	726.6	562.0	0.8158E-01	0.5544E-04	60 Bar
SPC-TraPPE Decane	B=1.20	500	721.3	550.7	0.1218	0.4213E-03	60 Bar, 500 water molecules
SPC-TraPPE Decane	B=1.30	500	720.7	551.0	0.1500	0.1372E-02	60 Bar, 500 water molecules
SPC-TraPPE Decane	B=1.40	500	715.7	546.4	0.2080	0.4155E-02	60 Bar, 500 water molecules
SPC-TraPPE Decane	L-B	550	638.9	551.8	0.1695	0.6026E-03	200 Bar
SPC-TraPPE Decane	B=1.20	550	630.6	538.7	0.2532	0.2842E-02	200 Bar, 500 water molecules
SPC-TraPPE Decane	B=1.30	550	621.8	531.9	0.3414	0.6773E-02	200 Bar, 500 water molecules
SPC-TraPPE Decane	B=1.40	550	580.1	524.2	0.4826	0.3873E-01	200 Bar, 500 water molecules
SPC-TraPPE Hexadecane	L-B	450	809.7	676.0	0.2532E-01	0.000	
SPC-TraPPE Hexadecane	B=1.20	450	813.9	674.4	0.3442E-01	0.000	500 water molecules
SPC-TraPPE Hexadecane	B=1.30	450	814.9	670.2	0.5323E-01	0.000	500 water molecules
SPC-TraPPE Hexadecane	B=1.40	450	811.3	672.5	0.6538E-01	0.000	500 water molecules
SPC/E-Karayannis Hexane	L-B (≈60)	450	866.0	73.99	0.1562	0.1600E-04	500 water molecules
SPC/E-Karayannis Hexane	L-B	450	866.3	219.0	0.4756E-01	0.2670E-04	60 Bar 500 water molecules
SPC/E-Karayannis Hexane TraPPE eps	B=1.50	450	872.8	461.0	0.5400E-01	0.3083E-02	500 water molecules
SPC/E-Karayannis Octane	L-B	450	--	--	--	--	500 water molecules
SPC/E-Karayannis Octane TraPPE eps	B=1.50	450	873.3	541.5	0.4899E-01	0.8977E-03	500 water molecules
SPC/E-Karayannis Decane TraPPE eps	B=1.50	350	964.7	674.7	0.1278E-02	0.000	500 water molecules
SPC/E-Karayannis Decane TraPPE eps	B=1.50	400	931.5	635.0	0.7659E-02	0.000	500 water molecules
SPC/E-Karayannis Decane	L-B	450	863.7	509.6	0.1785E-01	0.2349E-05	500 water molecules
SPC/E-Karayannis Decane TraPPE eps	L-B	450	866.4	591.5	0.1068E-01	0.9691E-05	500 water molecules
SPC/E-Karayannis Decane TraPPE eps	B=1.50	450	865.2	590.6	0.3518E-01	0.3791E-03	500 water molecules
SPC/E-Karayannis Decane TraPPE eps	80	450	864.9	590.8	0.1643E-01	0.6756E-04	500 water molecules
SPC/E-Karayannis Decane TraPPE eps	100	450	865.1	591.5	0.3408E-01	0.7063E-03	500 water molecules
SPC/E-Karayannis Decane	277.828 GROMOS	450	Complete	miscibility	of components		500 water molecules
SPC/E-Karayannis Decane	L-B	500	--	--	--	--	500 water molecules
SPC/E-Karayannis Decane	L-B	500	--	--	--	--	60 Bar 500 water molecules
SPC/E-Karayannis Decane TraPPE eps	B=1.50	500	813.0	545.5	0.1590	0.1941E-02	60 Bar 500 water molecules
SPC/E-Karayannis Decane	L-B	550	--	--	--	--	60 Bar 500 water molecules, vapourises
SPC/E-Karayannis Decane TraPPE eps	B=1.50	550	731.4	534.0	0.3504	0.5094E-02	200 Bar 500 water molecules
SPC/E-Karayannis Hexadecane	L-B	450	--	--	--	--	500 water molecules
SPC/E-Karayannis Hexadecane TraPPE eps	B=1.50	450	876.8	657.6	0.4531E-01	0.000	500 water molecules
SPC-Karayannis Hexane	L-B (≈60)	450	811.9	57.47	0.3792	0.4017E-04	500 water molecules
SPC-Karayannis Hexane TraPPE eps	L-B	450	808.4	455.9	0.3050E-01	0.1698E-03	500 water molecules
SPC-Karayannis Hexane TraPPE eps	B=1.20	450	807.5	453.3	0.4485E-01	0.1024E-02	500 water molecules
SPC-Karayannis Hexane TraPPE eps	B=1.30	450	804.1	450.7	0.5535E-01	0.2176E-02	500 water molecules
SPC-Karayannis Hexane TraPPE eps	B=1.40	450	800.0	446.3	0.7268E-01	0.5859E-02	500 water molecules

Models	*Epsilon O-C* *K*	*T* *K*	*Rho Waterbox* *kg/m³*	*Rho Alkanebox* *kg/m³*	*Solubility of water in alkane* *(mol%)*	*Solubility of alkane in water* *(mol%)*	*Comments*
SPC-Karayannis Octane	L-B	450	--	--	--	--	500 water molecules
SPC-Karayannis Octane TraPPE eps	B=1.20	450	822.9	536.3	0.4713E-01	0.1409E-03	60 Bar 500 water molecules
SPC-Karayannis Octane TraPPE eps	B=1.30	450	810.2	542.0	0.4709E-01	0.7241E-03	500 water molecules
SPC-Karayannis Octane TraPPE eps	B=1.40	450	808.4	533.3	0.6855E-01	0.1882E-02	500 water molecules
SPC-Karayannis Decane TraPPE eps	B=1.20	350	932.4	677.7	0.1923E-02	0.000	500 water molecules
SPC-Karayannis Decane TraPPE eps	B=1.30	350	936.1	676.3	0.2223E-02	0.000	500 water molecules
SPC-Karayannis Decane TraPPE eps	B=1.40	350	935.0	677.8	0.2449E-02	0.000	500 water molecules
SPC-Karayannis Decane TraPPE eps	B=1.20	400	879.2	636.5	0.8306E-02	0.000	500 water molecules
SPC-Karayannis Decane TraPPE eps	B=1.30	400	880.7	636.6	0.1145E-01	0.000	500 water molecules
SPC-Karayannis Decane TraPPE eps	B=1.40	400	879.8	636.3	0.1606E-01	0.000	500 water molecules
SPC-Karayannis Decane	L-B	450	809.5	502.4	0.4256E-01	0.2461E-05	500 water molecules
SPC-Karayannis Decane	80	450	813.8	501.6	0.7702E-01	0.2889E-03	500 water molecules
SPC-Karayannis Decane	100	450	773.3	498.8	0.1631	0.2258E-01	500 water molecules
SPC-Karayannis Decane TraPPE eps	L-B	450	812.0	588.6	0.2558E-01	0.1879E-06	500 water molecules
SPC-Karayannis Decane TraPPE eps	B=1.20	450	814.1	586.9	0.3867E-01	0.9911E-04	500 water molecules
SPC-Karayannis Decane TraPPE eps	B=1.30	450	808.4	590.2	0.4660E-01	0.2209E-03	500 water molecules
SPC-Karayannis Decane TraPPE eps	B=1.40	450	807.9	585.5	0.6587E-01	0.5442E-03	500 water molecules
SPC-Karayannis Decane TraPPE eps	B=1.50	450	803.2	586.7	0.8124E-01	0.4459E-02	500 water molecules
SPC-Karayannis Decane TraPPE eps	80	450	811.4	588.5	0.4079E-01	0.7437E-04	500 water molecules
SPC-Karayannis Decane TraPPE eps	100	450	801.5	587.2	0.9122E-01	0.4538E-02	500 water molecules
SPC-Karayannis Decane	L-B	500	--	--	--	--	60 Bar 500 water molecules
SPC-Karayannis Decane TraPPE eps	B=1.20	500	723.6	537.0	0.1332	0.4413E-03	60 Bar 500 water molecules
SPC-Karayannis Decane TraPPE eps	B=1.30	500	721.6	534.3	0.1628	0.1351E-02	60 Bar 500 water molecules
SPC-Karayannis Decane TraPPE eps	B=1.40	500	713.0	531.6	0.2354	0.4392E-02	60 Bar 500 water molecules
SPC-Karayannis Decane	L-B	550	--	--	--	--	200 Bar 500 water molecules
SPC-Karayannis Decane TraPPE eps	B=1.20	550	631.1	526.4	0.2635	0.2689E-02	200 Bar 500 water molecules
SPC-Karayannis Decane TraPPE eps	B=1.30	550	625.0	518.9	0.3530	0.6330E-02	200 Bar 500 water molecules
SPC-Karayannis Decane TraPPE eps	B=1.40	550	599.0	516.1	0.4878	0.2405E-01	200 Bar 500 water molecules
SPC-Karayannis Hexadecane	L-B	450	--	--	--	--	500 water molecules
SPC-Karayannis Hexadecane TraPPE eps	B=1.20	450	820.8	660.0	0.4855E-01	0.000	500 water molecules
SPC-Karayannis Hexadecane TraPPE eps	B=1.30	450	805.0	660.3	0.4984E-01	0.000	500 water molecules
SPC-Karayannis Hexadecane TraPPE eps	B=1.40	450	806.0	664.2	0.6661E-01	0.000	500 water molecules